Investigation of bound and unbound phosphoserine phosphatase conformations through Elastic Network Models and Molecular Dynamics simulations

Leherte, Laurence; Haufroid, Marie; Mirgaux, Manon; Wouters, Johan

Published in:
Journal of Biomolecular Structure & Dynamics

DOI:
10.1080/07391102.2020.1772883

Publication date:
2020

Document Version
Peer reviewed version

Investigation of bound and unbound phosphoserine phosphatase conformations through Elastic Network Models and Molecular Dynamics simulations

Laurence Leherte*, Marie Haufroid, Manon Mirgaux, Johan Wouters

Laboratoire de Chimie Biologique Structurale, Unité de Chimie Physique Théorique et Structurale, Department of Chemistry, NAmur Research Institute for LIfe Sciences (NARILIS), NAmur MEdicine & Drug Innovation Center (NAMEDIC), Namur Institute of Structured Matter (NISM), University of Namur, Rue de Bruxelles 61, B-5000 Namur (Belgium)

ORCID: L. Leherte 0000-0001-8468-5462
M. Haufroid 0000-0002-2816-992X
M. Mirgaux 0000-0002-6469-0552
J. Wouters 0000-0002-4920-6857

* Corresponding author
Email: laurence.leherte@unamur.be
LinkedIn: https://be.linkedin.com/in/laurence-leherte-10b53420

Abstract

The human phosphoserine phosphatase (hPSP) catalyses the last step in the biosynthesis of L-serine. It involves conformational changes of the enzyme lid once the substrate, phosphoserine (PSer), is bound in the active site. Here, Elastic Network Model (ENM) is applied to the crystal structure of hPSP to probe the transition between open and closed conformations of hPSP. Molecular Dynamics (MD) simulations are carried out on several PSer-hPSP systems to characterise the intermolecular interactions and their effect on the dynamics of the enzyme lid. Systems involving either Ca^{++} or Mg^{++} are considered. The first ENM normal mode shows that an open-closed transition can be explained from a simple description of the enzyme in terms of harmonic potentials. Principal Component Analyses applied to the MD trajectories also highlight a trend for a closing/opening motion. Different PSer orientations inside the enzyme cavity are identified, i.e., either the carboxylate, the phosphate group of PSer, or both, are oriented towards the cation. The interaction patterns are analysed in terms of hydrogen bonds, electrostatics, and bond critical points of the electron density distributions. The latter approach yields a global description of the bonding intermolecular interactions. The PSer orientation determines the content of the cation coordination shell and the mobility of the substrate, while Lys158 and Thr182, involved in the reaction mechanism, are always in interaction with the substrate. Closed enzyme conformations involve Met52-Gln204, Arg49-Glu29, and Arg50-Glu29 interactions. Met52, as well as Arg49 and Arg50, also stabilize PSer inside the cavity.

Keywords

Human phosphoserine phosphatase, elastic network model, molecular dynamics, promolecular electron density, critical points

List of abbreviations

AA, amino acid

AIM, atoms-in-molecules

com, centre-of-mass

CP, critical point

ED, electron density

ENM, elastic network model

Hbond, hydrogen bond

hPSP, human phosphoserine phosphatase

MD, Molecular Dynamics

NH3, positively-charged NH_3 group of PSer

NMA, normal mode analysis

PC, principal component

PCA, principal component analysis

PSer, phosphoserine

RDG, reduced density gradient

RMSD, root mean square displacement

RMSF, root mean square fluctuations

SR, short-range

Introduction

Human phosphoserine phosphatase (hPSP) is an effective enzyme in the phosphorylated pathway of serine biosynthesis, which catalyses the magnesium-dependent hydrolysis of L-phosphoserine (PSer) and controls the exchange between L-serine and L-phosphoserine (Collet et al., 1997). Defects in the biosynthesis of L-serine cause various serine-deficiency disorders (de Koning & Klomp, 2004; Brassier et al., 2016). Particularly, psychomotor retardments, severe tetraplegia, microcephaly, neurodegenerative disorders, and Williams syndrome have been observed (Tabatabaie et al., 2010; Jaeken, 2012). The serine pathway also sparks an interest in the cancer research (DeBerardinis, 2011; Yoon et al., 2015; Mullarky et al., 2016). Indeed, several studies highlight a link between the over-activation of the pathway and the cellular proliferation of tumoral cells (DeBerardinis, 2011; Mullarky et al., 2016). On the other hand, the overexpression of hPSP has also been linked to chemoresistance (Li et al., 2016; Sata et al., 2017).

The human enzyme has been purified and crystallised, and is reported to be inhibited by calcium (Peeraer et al., 2002; Peeraer et al., 2004). As suggested by Peeraer et al., the weak selectivity of hPSP towards ion size can originate from the presence of water molecules among the ligands (Peeraer et al., 2004). Moreover, the binding cavity of hPSP is large enough to accommodate various ion sizes and coordination patterns. More generally, Jing et al. conclude that a high number of charged residues in a binding pocket, such as aspartate and/or glutamate residues, tend to preferentially bind Ca^{++} (Jing et al., 2018). The lifetime of water molecules coordinated to Ca^{++} is expected to be lower than it is for Mg^{++}. In bulk water, it is estimated to be shorter than 20 ps and as long as hundreds of ps when bound to Ca^{++} and Mg^{++}, respectively (Jiao et al., 2006).

Based on the crystal structures of calcium and magnesium-containing hPSP bound to the substrate or the product of the reaction, our group recently published an interpretation of the reaction pathway of

hPSP (Haufroid et al., 2019). Closed and open forms of the hPSP were shown to occur depending upon the bound state of the enzyme. In the open conformation, the active site is available to the substrate, PSer, through a deconstruction of an α-helix involved in the residue sequence 40 to 56 located on the lid of the cavity, while in the closed form, that same helix is formed in the presence of the substrate (Peeraer et al., 2003; Haufroid et al., 2019).

In the present paper, the dynamics of hPSP lid is studied through Elastic Network Model (ENM) and Molecular Dynamics (MD) simulations to probe transitions between open and closed conformations as a function of the metal ion and the substrate orientation. A variety of hPSP systems are studied, involving either a calcium or a magnesium cation, complexed or not with PSer. To overcome energy barriers that may hinder the substrate mobility, different MD starting states are considered. The enzyme conformation and the ligand orientation and dynamics are interpreted in terms of interaction between the various components of the systems, i.e., the protein, the ligand, the metal cation, and the solvent molecules. Substrate-enzyme interactions are characterised using conventional techniques such as hydrogen bond (Hbond) and electrostatic concepts, combined with a topological analysis of the electron density (ED) distribution functions.

The Results section is organised as follows. First, the ENM results are discussed to interpret the experimental B-factors and verify, on a mechanistical point of view, the transition between open and closed forms of the enzyme. Second, a finer analysis of the enzyme dynamics and energetics is presented in the MD section B. In sub-section B.1, the hPSP dynamics is interpreted in terms of fluctuation profiles and correlated motions of the protein lid, regardless of the substrate. A novel descriptor of the covariance maps is proposed to highlight the most fluctuating domain of the enzyme. Different deformation patterns of the lid are illustrated. In sub-section B.2, the different orientations PSer can adopt inside the enzyme cavity are described in terms of the cation coordination degree. An emphasis is also given on the similarity between the location of persistent water molecules and crystal water molecules. Sub-section B.3 completes the substrate description by the analysis of its flexibility and the Hbonds it forms. In sub-section B.4, the structural information given in sub-sections B.2 and B.3 is completed by energetics considerations. The stabilising interactions are described using an original approach which combines the topological analysis of the electron density (ED) distribution function and descriptors of the so-called Non-Covalent Interaction (NCI) method. In the final sub-section B.5, the opening/closing motion of the enzyme lid is discussed in the frame of the equilibrium MD simulations to locate the structural elements that definitely characterise the closed form of the enzyme.

Materials and methods

To model the closed and open forms of hPSP, chains A and B of the hPSP-PSer crystal structure (PDB access code 6HYJ) were selected, respectively (Haufroid et al., 2019). They were used as such for the ENM calculations while their sequence was completed for the purpose of the MD simulations (supplemental material S1). In both conformations, the cavity lid contains residues 39 to 72 while the opposite part of the aperture includes residues 175 to 210 (Figure 1a). The enzyme cavity region involves alternating layers of charged species, i.e., positive arginine residues 49, 50, 65, and 202, negative phosphate and carboxylate in PSer as well as its positive NH3 group, a positive metal cation, and negative aspartate residues 20, 22, 179, and 183 (Figure 1b). A positively-charged lysine, Lys158, is also present at the level of the active site.

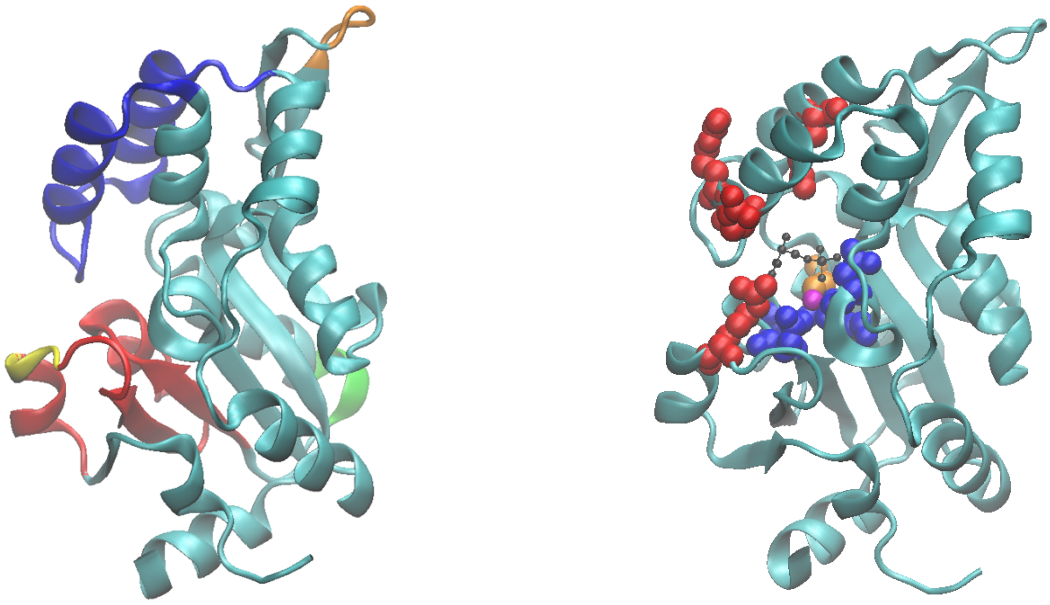

(a) (b)

Figure 1. Structure of hPSP taken from the chain A of the crystal structure hPSP-PSer. (a) Sequences 39 to 72 (blue), 175 to 210 (red), 138 to 141 (orange), 167 to 170 (green), 202 to 204 (yellow) are highlighted. (b) Calcium (magenta sphere), PSer (black sticks-and-balls), arginine (red spheres), aspartate (blue spheres), lysine (orange spheres).

A. Elastic Networks Models

ENM calculates the 3N-6 normal modes of vibration of a protein structure described using a limited set of N masses. Usually, each amino acid (AA) residue is represented by one grain, placed at the Cα location. All Cα atoms interact with each other depending upon their separation distance, through an interaction potential which, in its simplest form, mimics a harmonic spring. The Hessian matrix is diagonalised and the eigenvalues (vibration frequencies), as well as the eigenvectors (displacement vectors associated with the vibration modes), are obtained to yield information such as B factors, correlation matrices between the mobile entities, and deformation pathways from a conformation to another. The calculations were carried out with the web server iMods (López-Blanco et al., 2014). To describe the Cα-Cα interactions, the edNMA model was selected (Orellana et al., 2010). It is based on Cα-Cα force constants that were determined from MD trajectories of various protein systems and does not require any user-specified cut-off values. We applied the software to evaluate B-factors and to model the transition between the open (chain B) and closed (chain A) forms of hPSP whose structures have been described previously (Haufroid et al., 2019).

B. Molecular Dynamics simulations

Details regarding the technical aspects of the structure building and the 200 ns MD simulations are provided in the supplemental materials S1 and S2, respectively. The systems were modelled using the force field Amber99sb-ildn (Lindorff-Larsen et al., 2010) and MD simulations were carried out at 300 K and 1 bar with the program Gromacs4.5.5 (Hess et al., 2008; Pronk et al., 2013). The 'V-rescale' and 'Parrinello-Rahman' algorithms were selected to constrain P and T, respectively. A number of systems were studied as summarised in Figure 2. Particularly, the crystal chain A containing PSer and Ca^{++} was investigated from two different starting states. The corresponding MD trajectories are named A/Ca/PSer and A_w/Ca/PSer, respectively. The subscript *w* means that crystal water molecules are considered in the starting system. Three simulations with a magnesium ion in the presence of PSer were also carried out using different starting points, i.e., A/Mg/PSer, A_c/Mg/PSer, and A_{cw}/Mg/PSer. In A/Mg/PSer, the crystal structure of the system is considered with Mg^{++} replacing Ca^{++}. In A_c/Mg/PSer and A_{cw}/Mg/PSer, the final frame of simulations A/Ca/PSer and A_w/Ca/PSer are considered as the starting points of the magnesium-dependent MD simulations, respectively. The subscript *c* stands for "continuation". Finally, two simulations of the magnesium-containing enzyme were carried out without any substrate. Their starting state is the last frame of the simulations

A_c/Mg/PSer and A_{cw}/Mg/PSer, respectively. Simulations with Ca^{++} and Mg^{++} were both carried out as the system is known to be more reactive with Mg^{++} than with Ca^{++} (Peeraer et al., 2004) while simulations without the substrate were achieved to complement the analysis of the enzyme lid conformation. Simulations of hypothetical open systems built with chain B complexed to the substrate were also considered, with either calcium or magnesium ions. To place the substrate in the chain B, the crystal structure of chain A and PSer was aligned onto the crystal structure of chain B (Figure S1, supplemental material). The simulations are called B/Ca/PSer and B/Mg/PSer. Two simulations of the chain B were also carried out without any substrate (simulations B/Ca and B/Mg).

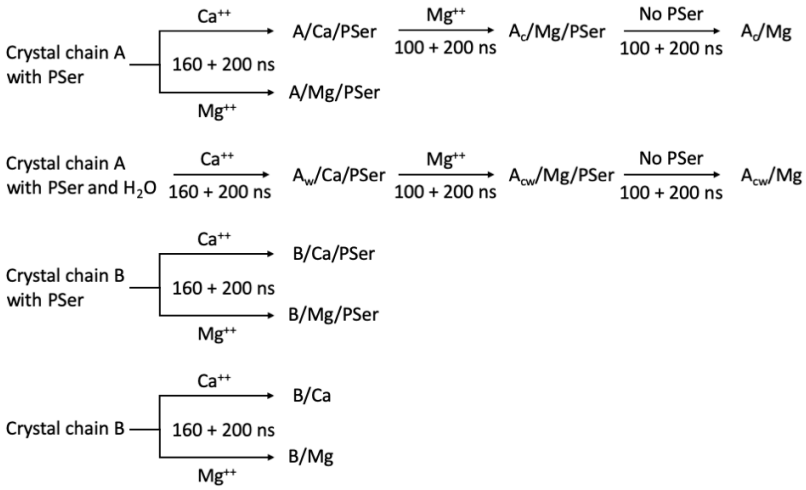

Figure 2. Description of the MD simulation strategy to simulate solvated hPSP systems.

C. Critical point analysis of the electron density distribution

In his Atoms-in-Molecules (AIM) theory, Bader defined a molecular system as a set of atomic basins, each characterised by a maximum in the ED (Bader, 2001). The contact area of two basins that are associated with two atoms coincides with a bond critical point (CP) or pass (saddle point). CPs are points where the gradient of the ED distribution is zero. Four kinds of CPs can be identified, based on the number of negative eigenvalues of their corresponding Hessian matrix (a matrix built on the second derivatives of the ED) (Figure S2, supplemental material). A peak or maximum in the ED is characterised by 3 negative eigenvalues (e_1,e_2,e_3), noted (-,-,-). A pass is defined by the set of signs (-,-,+), i.e., the second eigenvalue is negative too. It is located between two peaks, not necessarily covalently bound. The last two kinds of CPs, the pales (ring CPs) and pits (cage CPs), are described by the eigenvalue signs (-,+,+) and (+,+,+), respectively, i.e., the second eigenvalue is positive. In the Non-Covalent Interaction (NCI) approach, the ED is analysed so as to identify extended regions of

space where the reduced density gradient (RDG) function *s(**r**)* approaches zero (Johnson et al., 2010; Boto et al., 2015):

$$s(\boldsymbol{r}) = \frac{|\nabla\rho(\boldsymbol{r})|}{2(3\pi^2)^{1/3}\rho(\boldsymbol{r})^{4/3}} \qquad (1)$$

In such regions, bonding and non-bonding interactions are characterised by negative and positive second derivatives e_2 of $\boldsymbol{H}$, respectively.

Previously, we described an algorithm to locate the peaks in an ED distribution function expressed as a summation over atomic Gaussian functions (Leherte, 2004). We have extended the approach to locate the other kinds of CPs using the iterative refinement relationship:

$$\boldsymbol{r}_{CP(\mathrm{n+1})} = \boldsymbol{r}_{CP(\mathrm{n})} - \delta\, \boldsymbol{H}_n^{-1}\, \nabla\rho(\boldsymbol{r}) \qquad (2)$$

where $\boldsymbol{r}$ is the position vector of the refined CP, n is the iteration step, δ is the allowed displacement, and $\boldsymbol{H}_n$ is the Hessian matrix at step n. Particularly, the starting points for the search of the peaks and passes of an ED distribution function are the atoms and all atom-atom mid-distance points, respectively. The refinement process stops when a lower limit for $|\nabla\rho(\boldsymbol{r})|$, 10^{-7} e/bohr^4, is reached.

In the present work, the molecular ED distribution function *ρ(**r**)* is a summation over independent atomic contributions whose parameters are obtained using a Fourier transformation of the Cromer-Mann scattering factors (Ibers & Hamilton, 1974) (Table S3, supplemental material). Within such a promolecular ED description, all atoms are neutral except the metal cation. Several studies have emphasized the very small differences between promolecular and quantum-mechanical ED distribution functions (Gironés et al., 2001; Johnson et al., 2010). Working with promolecular ED representations is thus a logical choice to limit the time of the ED calculation. To further reduce the computation time, the ED is calculated using only the cation, the substrate atoms, and all hPSP residues atoms having at least one atom located at a distance ≤ 1 nm from PSer.

Results

A. Elastic Networks Models

The first vibrational mode, depicting the largest fluctuations of each conformation, is presented in the supplemental Figure S3. The predicted B-factors, calculated from all eigenvectors and eigenvalues of the NMA decomposition scheme are reported in Figure 3a.

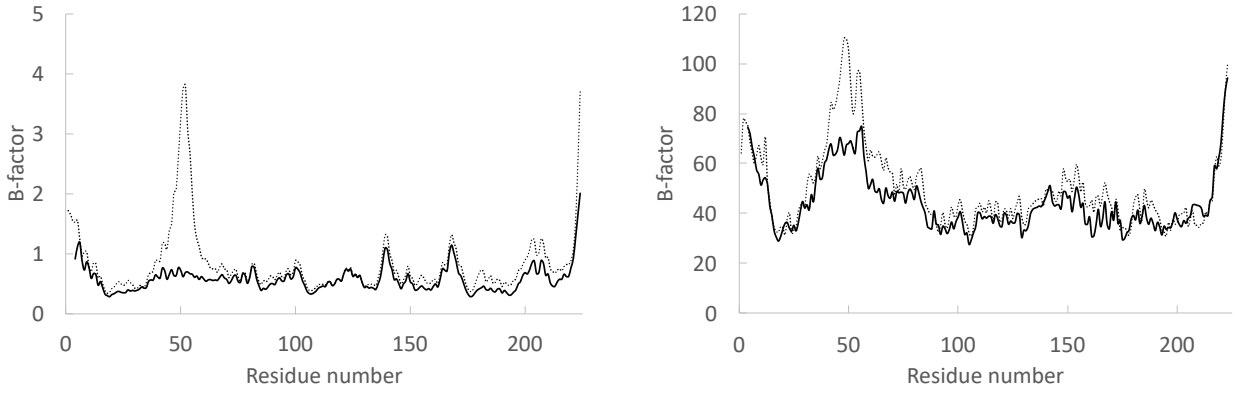

(a) (b)

Figure 3. (a) iMods predicted B-factors of chains A (plain line) and B (dotted line) as taken from the crystal complex PSer-hPSP. (b) Experimental B-factors of chains A (plain line) and B (dotted line).

Apart from the chain ends, the most mobile AA sequences of the closed form of hPSP are located at residues 138 to 141 and 167 to 170 (Figure 1). Residues 202 to 204, which are part of one side of the cavity aperture, present a slightly lower mobility. The correlation matrices built from the displacement of the Cα atoms show a negative correlation between their motion and the other side of the cavity aperture, i.e., Met52 (Figure S4, supplemental material).

The residues of the cavity lid are not seen as highly mobile due to the numerous interactions they form with the rest of the enzyme compared to the open form. The experimental B factors show a similar trend (Figure 3b). In the open form, residues 40 to 63, which are part of the cavity lid, clearly form the most mobile segment of the protein due to the loss of close contacts with neighbouring residues. ENM thus suggests that the opening of the lid is energetically less favoured than its closure due to the more numerous network springs to be deformed. At the all-atom level, a structure analysis of the hPSP lid residues, carried out using the Web server RING2.0.1 (Piovesan et al., 2016), provides details regarding the interactions involved by the residues 40 to 56 of the hPSP lid (Figure S5, supplemental

material). In the open form, the number of hydrogen bonds (Hbonds) occurring between the lid residues is limited due to the deconstruction of the helix in the AA sequence 40 to 56. In chain A, Met52 is identified as forming Hbonds with two residues located outside the lid, Glu29 and Arg202, while it is not involved in any particular contacts in chain B. In that last conformer, two small clusters depict pairs of residues which are not identified as interacting with the rest of the enzyme.

The transition pathways between the open and closed forms of hPSP, and inversely, modelled using the first 10 % of the normal modes generated with iMods, are displayed in Figure 4. The initial RMSD value between the Cα atoms of the A and B crystal structures is 0.26 nm. The final RMSD values, 0.18 and 0.12 nm, indicate the quality of the fit between the deformed conformation of the starting hPSP structure and the target conformation. In the first case, i.e., the morphing of chain A to chain B, the distance between residues 52 and 202 ranges from 10.03 to 18.77 Å, while in the second case, it spans distance values from 22.54 to 6.78 Å. The larger difference between the two last values is explained by the higher mobility of the cavity lid of chain B, whose Cα atoms are constrained by a limited number of close neighbours, as also seen in the all-atom structure (Figure S5, supplemental material).

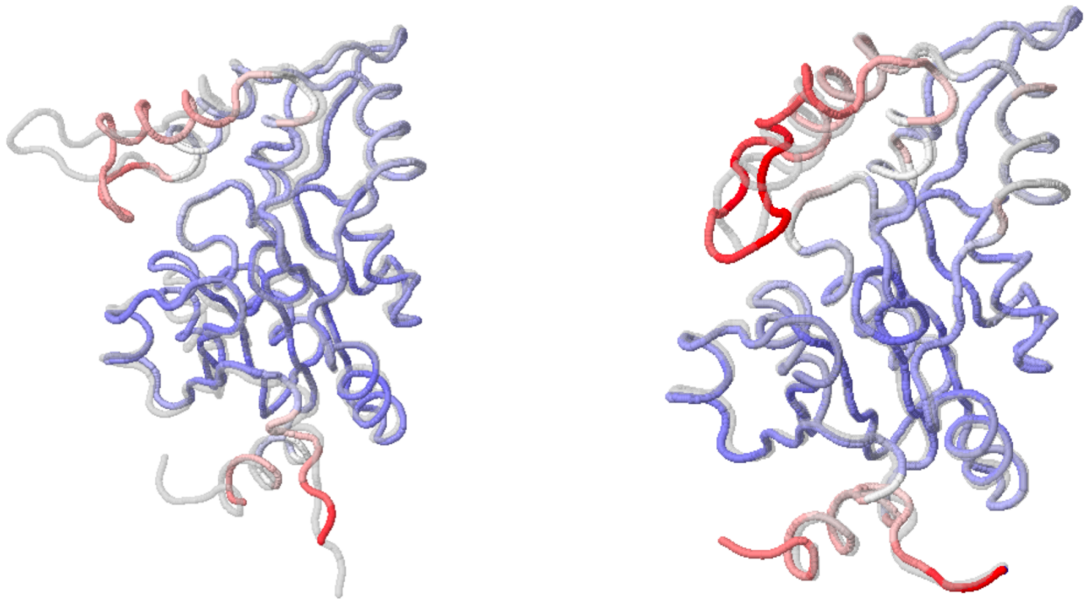

(a) Chain A (coloured) to chain B (gray) (b) Chain B (coloured) to chain A (gray)

Figure 4. Superimposition of the maximal predicted deformation of (a) chain A and (b) chain B of hPSP as generated using iMods (López-Blanco et al., 2014). The colour intensity reflects the mobility degree (from blue to red).

In conclusion, a simple ENM is sufficient to explain the closure, or the opening, of the hPSP lid using a limited amount of normal modes. Closure appears to be fully explained by NMA while opening is a more hindered movement. Even if the precise time scale over which the phenomenon occurs is not evaluated, NMA provides an informative view of slow movements. However, ENM modelling does not include finer interaction effects like those involving a ligand, a metal cation, and the solvent. MD simulations allow to more deeply investigate the properties of a confined ligand interacting within the enzyme cavity, and the specific interactions occurring at the level of the cavity lid upon opening/closure of the hPSP conformation.

B. Molecular Dynamics simulations

The analysis of the MD trajectories especially focuses on the deformation of the hPSP enzyme, sampled through chemically and conformationally different systems. In that frame, the occurence of open and closed conformations is characterised in terms of cation coordination, ligand orientation, and specific interactions.

B.1. Overall dynamics and conformational analysis of hPSP

Time-dependent Root Mean Square Displacement (RMSD) values calculated from the initially optimised conformation of the system are all below 0.4 nm (Figure S6, supplemental material). The profiles of the systems A/Mg/PSer and B/Ca/PSer present a steep variation, around 185 ns and 187 ns, respectively. In A/Mg/PSer, the RMSD decreases from 0.33 to 0.29 nm in about 3.8 ns, and is related to the definite closure of the enzyme lid as discussed in Section B.5. For the system B/Ca/PSer, the RMSD varies from 0.30 to 0.37 nm between 186.8 ns and 189.0 ns. It corresponds to a slight and temporary opening of the enzyme structure triggered by a flip of the Arg50 side chain which finally build interactions with the substrate (see Section B.4).

The Root Mean Square Fluctuation (RMSF) profiles clearly show that the loop 40-56 is characterised by the largest fluctuations, as also evidenced in the experimental data (Figure 3b) and in ENM results (Figure 3a), regardless of the presence of the substrate or the nature of the cation (Figures 5 and S7). It is particularly clear for Met52 in the enzyme complex A/Ca/PSer with a RMSF value of 0.50 nm. Fluctuations of the enzyme lid are lowered when crystal water molecules are considered in the starting state of the chain A simulation (Figure 5a) and in the presence of Mg^{++}, except for the system A/Mg/PSer wherein the magnesium ion is screened by two water molecules as further detailed in the text (Figure S7b, supplemental material). In magnesium-containing chains B, the RMSF profile of the

lid appears as a double-peak, with a minimum at residue Met47, regardless of the presence of the substrate (Figures 5b and S7d). Met47 is found to be constrained by its interaction with Arg65. Contrarily, in the open experimental conformation, Met47 is free to move (Figure 3b). Such a clear split of the RMSF values characterising the enzyme lid does not occur in chain A-based systems wherein the AA sequence 40-56 remains constrained by the more numerous interactions it forms with the enzyme.

Since the inspection of the RMSD profiles is not sufficient to detect conformational transitions of hPSP, a Principal Component Analysis (PCA) was applied to the covariance matrices of the Cα atom positions calculated over the 200 ns MD trajectories. Briefly, a PCA is intended to design a new reference system for a MD trajectory such as it maximises the variance of the data along each axis. It is achieved through a diagonalisation of the covariance matrix of the Cα atom positions which yields the corresponding eigenvalues (the fluctuation magnitude) and eigenvectors (the vectors depicting the direction of the atom fluctuations). It aims at characterising the extent of the conformation space that is accessed by the system during the simulation time (Baron et al., 2006). Usually the first two or three modes are sufficient to take into account the largest fluctuation motions, i.e., those involving the enzyme lid in the present work. The lid mobility can be largely explained using the first principal component (PC) only.

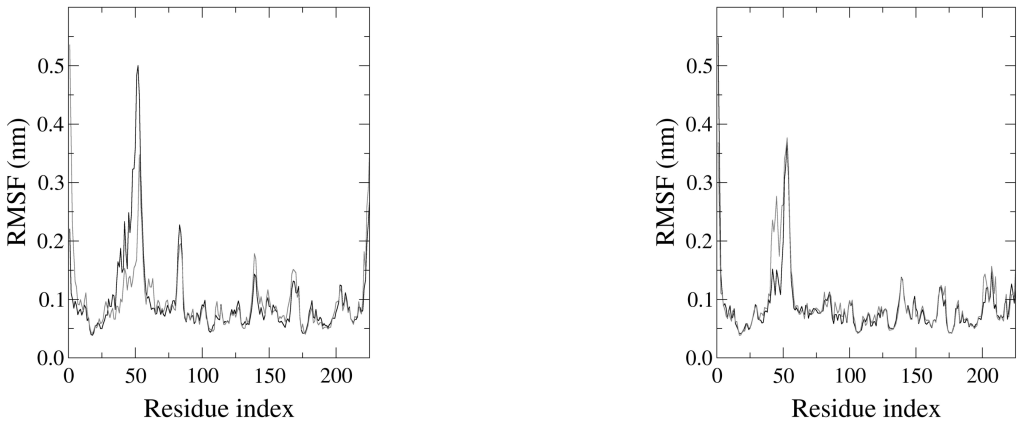

(a) A/Ca/PSer (black), A_w/Ca/PSer (grey) (b) B/Ca (black), B/Mg (grey)

Figure 5. RMSF of the hPSP Cα atoms as calculated from the last 200 ns of MD trajectories at 300 K and 1 bar.

To illustrate that particular point, a correlation factor κ_{ij} between the first time-dependent PC and the time-dependent $C\alpha_i$-$C\alpha_j$ distance profile d_{ij} was calculated using:

$$\kappa_{ij} = \left[\frac{1}{N_f}\sum_{n=1}^{N_f}(PC_n\ d_{ij,n}) - \overline{PC}\ \overline{d_{ij}}\right]\frac{1}{\sigma_{PC}\ \sigma_{d_{ij}}} \qquad (3)$$

where N_f is the number of time frames considered in the calculation, and $\bar{X}$ and σ_X stand for the mean and standard deviation of X calculated over the N_f frames, respectively. Then, the absolute value of κ_{ij} is multiplied by the largest range of distances, $\Delta d_{ij} = d_{ij,max}$-$d_{ij,min}$, so as to visually emphasise large amplitude motions that are correlated with the PC (Figures 6a and S8a). The $|\kappa_{ij}\Delta d_{ij}|$ maps clearly show that the distances involving residues located at the lid extremity are the most variable ones and are well correlated with the first PC. The same is also observed for shorter and stabilised trajectory elements, except for the simulations A_{cw}/Mg/PSer and B/Mg/PSer (Figure S8b, supplemental material). Particularly, the corresponding maps established during the last 100 and 75 ns, respectively, involve enzyme conformations where the lid is stabilised through an Arg49-PSer or an Arg50-PSer interaction, respectively, as detailed in Section B.4.

The correlation values κ_{ij} calculated between the Cα52-Cα202 distance and the first PC are reported in Table 1.

Table 1. Correlation index κ_{ij} [a] calculated between $C\alpha_i$-$C\alpha_j$ distances and the first PC, as obtained from the last 200 ns of MD trajectories at 300 K and 1 bar.

	Cα52-Cα202	Cα39-Cα52	Cα54-Cα202
A/Ca/PSer	**-0.87**	0.47	-0.18
A_w/Ca/PSer	-0.13	-0.56	**-0.75**
A_c/Mg/PSer	0.40	0.26	**0.66**
A_{cw}/Mg/PSer	**0.77**	-0.79	-0.04
A/Mg/PSer	**-0.88**	0.26	-0.06
A_c/Mg	0.21	**-0.56**	0.37
A_{cw}/Mg	**0.72**	0.41	0.41
B/Ca	**-0.71**	0.49	-0.61
B/Mg	**-0.60**	-0.05	0.28
B/Ca/PSer	-0.42	-0.12	**-0.95**
B/Mg/PSer	-0.08	**-0.60**	-0.13

[a]The largest absolute values of κ_{ij} are in bold.

For several MD simulations, an absolute correlation value κ_{ij} above 0.6 confirms that the largest displacement, reflected by the first PC, is associated with the lid closure described by the distance Cα52-Cα202. For the system A_c/Mg/PSer, an intermediate value of 0.40 is calculated, while a larger correlation, 0.66, is actually obtained with the distance Cα54-Cα202. The lowest correlation values, around or below an absolute value of 0.2, can only be increased if one focuses on the Cα39-Cα52 distance which describes the shortening of the lid. In the particular case of the systems B/Mg/PSer, the

first PC is actually correlated to the deconstruction of the 39-44 loop with a correlation index of 0.75 between the distance Cα39-Cα44 and the first PC. As an illustration, new trajectories generated using the first PC for the systems A/Ca/PSer and A_c/Mg are given in Figure 6b which highlights different deformation modes. In A/Ca/PSer, an increase of the aperture width is observed. In A_c/Mg, the deformation is limited to the tip residues of the lid, while in B/Mg/PSer where the initial aperture is larger, the lid extremity is largely distorted. It is also observed that the largest eigenvalue of each system, λ_1, adopts the smallest value, below 0.6 nm^2, in the absence of the substrate (Table S4, supplemental material). It depicts limited conformation changes compared to enzymes bound to the substrate. All calcium-dependent systems have a higher λ_1 value than their corresponding magnesium-based complex. Their slowest motion is thus characterised by a larger magnitude. As an example, λ_1 that is associated with A/Ca/PSer and A/Mg/PSer is equal to 1.110 and 0.726 nm^2, respectively.

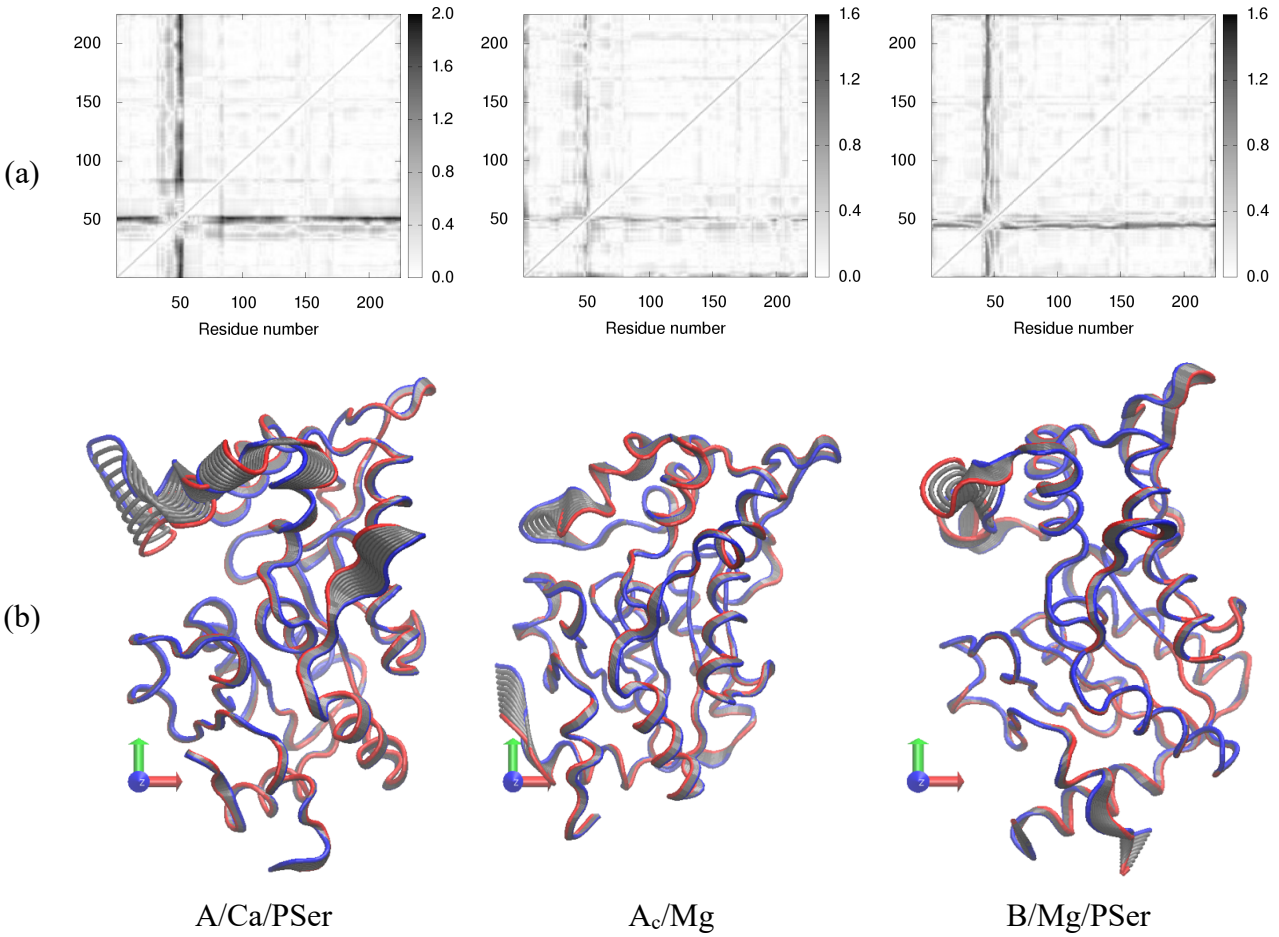

Figure 6. (a) $|\kappa_{ij}.\Delta d_{ij}|$ maps calculated using the first PC. Both axes report the residue index number. (b) hPSP motion modelled using the first PC of the Cα covariance matrix, obtained from the last 200 ns of MD trajectories at 300 K and 1 bar. Limit conformations are displayed in red and blue, eight intermediate conformations are displayed in grey.

B.2. Ion coordination and persistent water molecules

The cavity of hPSP involves a set of several negatively-charged aspartate residues, Asp20, Asp22, Asp179, and Asp183, all placed in a single hemisphere surrounding the metal ion, opposite to the cavity lid. Experimentally, Asp22 is the only one to share its backbone O atom in the coordination sphere of the metal cation (Haufroid et al., 2019). Due to their size, Mg^{++} and Ca^{++} are expected to be coordinated by 6 and 7 to 8 oxygen atoms, respectively (Peeraer et al., 2004). In the work achieved by Haufroid et al., the calcium ion of chain A of the enzyme bound to the substrate L-phosphoserine, is surrounded by eight oxygen atoms (Table S5, supplemental material). Their number reduces to six when one considers distances below 0.24 nm (see Table 4 in Peeraer et al., 2004). In MD simulations, the number of closest neighbours to the metal ion is obtained by integrating the first peak of the cation-oxygen radial distribution functions, with a distance cut-off of 0.35 (Wang et al., 2008) and 0.25 nm for Ca^{++} and Mg^{++}, respectively. Table S5 reveals that the number of closest neighbours to Mg^{++} is always 6, while it varies between 8 and 9 in the presence of calcium.

In chain A, Asp20 acts as a bidentate in the presence of Ca^{++} while it tends to act as a monodentate in magnesium-containing enzymes (Table S5, supplemental material), consistently with the observations reported by Peerear et al. (Peeraer et al., 2004). According to the authors, it explains the loss of reactivity of Asp20 when bound to a calcium ion. In chain B, Asp20 is also seen as a monodentate ligand, even in the presence of Ca^{++} now coordinated by water oxygen atoms rather than by atom OD1 of Asp20. Additionally, Asp22 is not coordinated to the magnesium ion any longer in the presence of PSer, as seen in simulation B/Mg/PSer. Rather, the PSer oxygen atoms displace the Asp22 atoms observed in simulations B/Ca and B/Mg (Table S5, supplemental material). In their paper, Haufroid et al. showed that Asp22 coordinates the metal ion of the enzyme through its main chain oxygen atom (Haufroid et al., 2019). Similarly, the MD simulations carried out with a calcium ion illustrate that O of Asp22 is involved in the coordination shell of PSer. MD simulations also suggest that Asp183, as well as PSer, can possibly belong to the coordination sphere of the Ca^{++} ion, which was however not reported in the experiments (Peeraer et al., 2004; Haufroid et al., 2019). Particularly, the simulations B/Ca and B/Mg indicate that, in the absence of the substrate, both OD1 and OD2 atoms of Asp183 coordinate the cation, contrarily to chain A.

As further described in Section B.3, the coordination shells of the metal ion reveal that the ligand can adopt four metal-binding patterns in the enzyme cavity. Either it interacts with the phosphate group of PSer, such as in simulations A_w/Ca/PSer, A_{cw}/Mg/PSer, and B/Mg/PSer, or with the carboxylate group of PSer, as in A/Ca/PSer and A_c/Mg/PSer (Figure 7). A bridged position, where the phosphate and carboxylate groups of PSer are both oriented towards the cation, is detected in the system B/Ca/PSer.

Finally, in A/Mg/PSer, two water molecules prevent PSer from being part of the coordination shell of Mg^{++}.

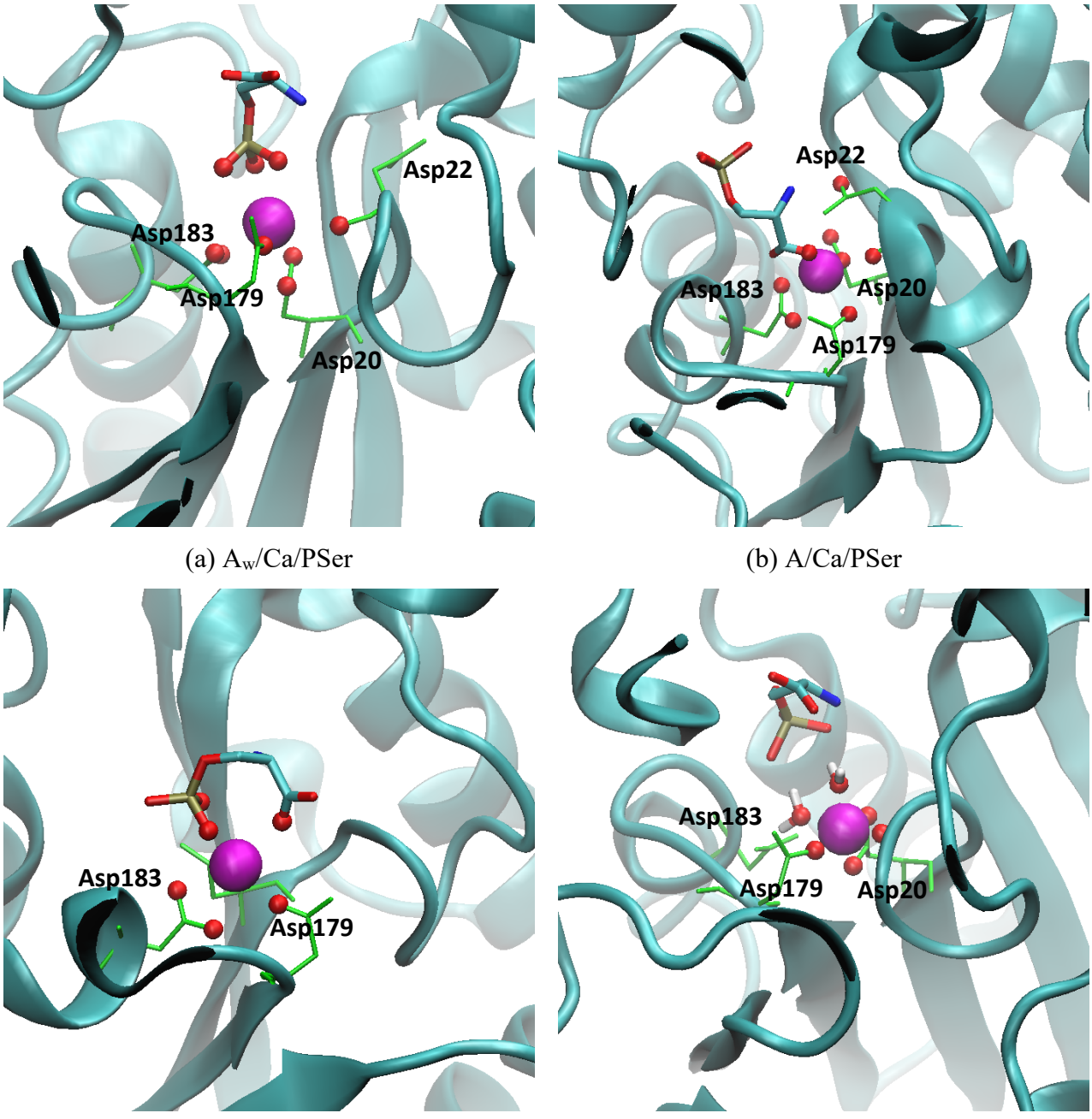

(a) A_w/Ca/PSer (b) A/Ca/PSer

(c) B/Ca/PSer (d) A/Mg/PSer

Figure 7. Final snapshots focussing on the cation coordination of the hPSP-PSer complexes as obtained from the last 200 ns of MD simulations at 300 K and 1 bar. The coordinated oxygen atoms and the cation are displayed using red and magenta spheres, respectively. Labelled amino acids are shown in green. H atoms are not shown for clarity.

The RMSF values of the oxygen atoms that are coordinated to the cation show great differences depending upon the nature of the cation and the origin of the oxygen atoms. The least mobile O atoms

are those of the aspartate residues of hPSP (Table S6, supplemental material). Their clearly lower O mobility observed in the presence of Mg^{++} might explain the higher activity of the magnesium-dependent enzyme. PSer O atoms also have a lower mobility in the presence of magnesium. Contrarily, the behaviour of water molecules coordinated to the metal cation is more variable and no specific trend is observed in the present study.

Permanent water sites are found at three different locations, i.e., either coordinated to the metal cation as in A/Mg/PSer (Figure 7d and Table S5 of the supplemental material), or in interaction with the hPSP sequence 179 to 202 (location II, Figure 8 and Table S7 of the supplemental material). In that last case, two water sites are observed at location II. An additional site, location III, is observed at the proximity of residues 133-134, 146-147, 150, and 153, which shape a small pocket, as in the systems A/Ca/PSer, A_c/Mg/PSer, A_{cw}/Mg/PSer, A_c/Mg, A_{cw}/Mg, B/Ca/PSer, and B/Mg/PSer (Figure 8).

When Ca^{++} is involved, water molecules at location I tend to be more often exchangeable compared to magnesium-containing complexes. Their occurrence frequency does not exceed 13 % of the simulation time in the case of simulation A/Ca/PSer, while in the presence of Mg^{++}, the two coordinated water molecules are observed all along the last 200 ns of the A/Mg/Pser and A_{cw}/Mg trajectories (Table S5, supplemental material). In the particular case of A/Mg/Pser, the two water molecules do not form any Hbond with each other and are seen as a screen between the substrate and the metal ion (Figure 7d). The largely negative water-cation interaction energy corroborates the persistent character of the water molecules (Table S8, supplemental material). Particularly, in both systems characterised by two permanent water molecules, A/Mg/PSer and A_{cw}/Mg, the short-range (SR) cation-H_2O interaction energy values are lower than -400 kJ/mol. The system B/Ca/PSer is the only exception with a positive mean SR cation-H_2O interaction energy value in the presence of one persistent water molecule, i.e., 70.18 ± 30.43 kJ/mol (Table S8, supplemental material).

At location II, two water molecules are Hbonded to either Asp179, Phe196, Val200, and Arg202, or to Phe196 and Val200, respectively. Both water sites are found in the crystal structure of chains A and B, and are almost systematically occupied by a water molecule in all MD simulations (Table S7, supplemental material).

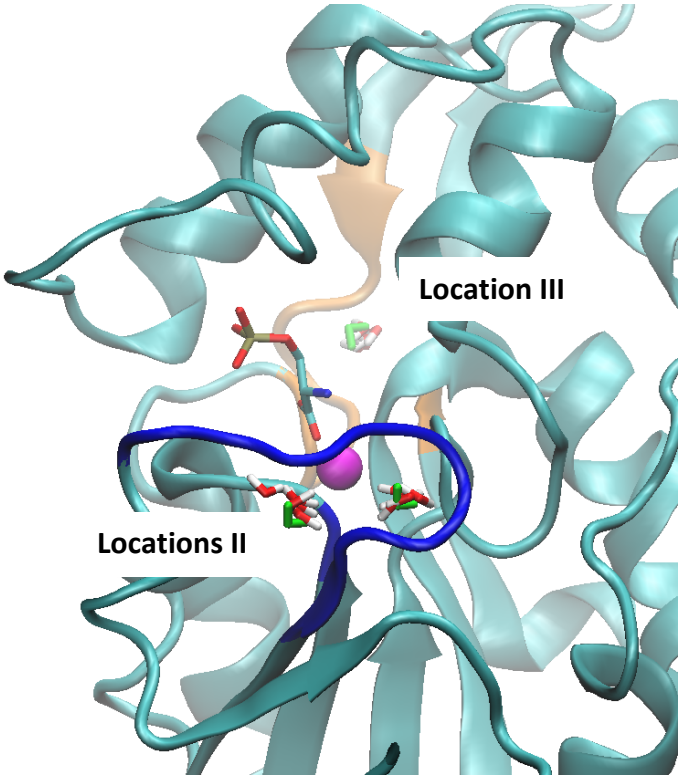

Figure 8. Snapshot at t = 100 ns of the system A_c/Mg/PSer as obtained from the last 200 ns of MD simulations at 300 K and 1 bar. Water molecules at locations II and III (shown at t = 100, 150, 200, 250, and 300 ns) are displayed together with Mg^{++} (magenta sphere) and PSer (sticks). Residues 179 and 196 to 204, and residues 133, 134, and 146 to 153 are shown in dark blue and orange, respectively. Corresponding crystal water molecules, obtained from a superimposition with the crystal structure of the chain A, are shown in green.

B.3. Substrate orientation and flexibility

In the crystal structure of the chain A of hPSP, the ligand is close to Asp20 (OD1-O2P = 0.26 nm), Met52 (SD-OXT = 0.15 nm), Phe58 (CZ-O1P = 0.43 nm), Lys158 (NZ-O2P = 0.12 nm), and Thr182 (OG1-O = 0.30 nm). A salt bridge is also found between Lys158, like in the artificially built PSer-Chain B complex (Figure S1, supplemental material), and the phosphate group of Ser while Met52 is involved in a close contact with the carboxylate group. The substrate PSer adopts a bridged orientation in interaction with the metal cation (Figure 9), with relatively similar distance values between the metal ion and the centre-of-mass (com) of the phosphate and carboxylate groups, i.e., 0.51 and 0.47 nm, respectively.

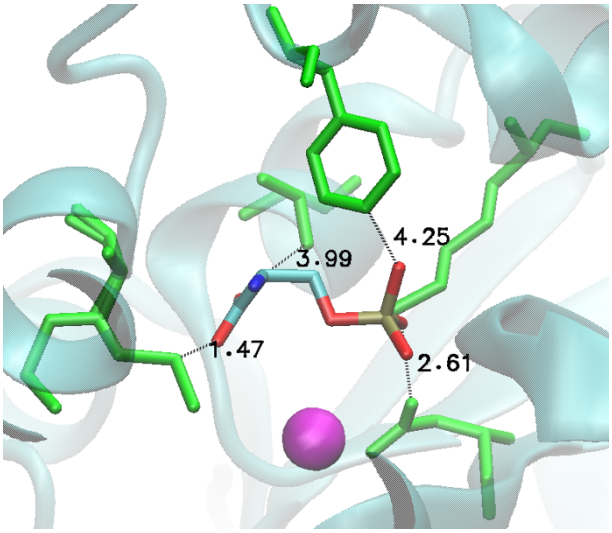

Figure 9. Crystal structure of chain A showing close contacts between the substrate (sticks) and hPSP (cyan ribbon). Ca^{++} and the residues Asp20, Met52, Phe58, Lys158, and Thr182, are displayed in magenta and green, respectively. Distance values are in Angströms.

As already mentioned in Section B.2, PSer can adopt different orientations inside the cavity (Table S5, supplemental material). Particularly, in the simulation A/Ca/PSer (Figure 7b), its carboxylate group is oriented towards the cation, at a distance of 0.35 ± 0.02 nm. Contrarily, when crystal water molecules are considered in the starting state (Figure 7a), its phosphate group is close to Ca^{++}, at a distance 0.29 ± 0.02 nm. Similarly to calcium-containing systems, PSer can adopt various orientations when it interacts with Mg^{++}, such as in systems A_c/Mg/PSer and A_{cw}/Mg/PSer. Thus, for the simulation times considered in the present work, energy barriers within the enzyme cavity are large enough to prevent orientation changes. As the substrate is closer to the magnesium cation than it is to Ca^{++}, its phosphate group is consequently closer to Asp 20 and Asp22 which are involved in the catalytic mechanism of dephosphorylation. The cation acts as a strong anchor to the substrate which is thus characterised by a low mobility. The bridged orientation detected in the simulation B/Ca/PSer is characterised by similar phosphate-cation and carboxylate-cation distances of 0.33 ± 0.01 and 0.36 ± 0.01 nm, respectively.
In the system A/Mg/PSer, two screening water molecules limit the cation-phosphate distance to 0.47 nm. The screening effect of water is clearly observed in the simulation A/Mg/PSer with a cation-PSer interaction energy value of only -117.97 ± 26.34 kJ/mol (Table S8, supplemental material), while the number of Hbonds PSer can form with water molecules is the highest, with a value of 14.6 ± 1.5 (Table 2). In the two other magnesium-based system, A_c/Mg/PSer and A_{cw}/Mg/PSer, the distance between the com of PSer groups and Mg^{++} can be as low as 0.2 nm, in agreement with the coordination sphere of the ion. This second state is most likely the one of interest in the activity of hPSP (Peeraer et al., 2003).

Table 2. Mean number of Hbonds[a] and standard deviation formed by PSer with water and hPSP as obtained from the last 200 ns of MD simulations at 300 K and 1 bar.

	A/Ca/PSer	A_w/Ca/PSer	A_c/Mg/PSer	A_{cw}/Mg/PSer	A/Mg/PSer	B/Ca/PSer	B/Mg/PSer
PSer-H_2O	11.5 ± 1.5	10.4 ± 1.5	7.0 ± 1.3	10.0 ± 1.9	14.6 ± 1.5	6.8 ± 1.1	10.2 ± 1.7
PSer-hPSP	5.6 ± 1.2	2.6 ± 1.1	10.0 ± 1.5	2.6 ± 1.3	2.9 ± 1.1	5.6 ± 0.8	2.3 ± 1.3

[a]Hbonds are determined based on cutoff values for the angle hydrogen-donor-acceptor (30°) and the distance donor-acceptor (0.35 nm).

As illustrated by the re-orientation correlation function C(t), PSer is the most flexible when the ion is screened, i.e., in the system A/Mg/PSer (Figure S9, supplemental material). Such functions are calculated as the first-order Legendre polynomial of the time-dependant angle of a vector normal to a plane defined by the ligand atoms N, C, and P. Correlation times τ were calculated by fitting C(t) between 1 and 5 ns using a single exponential function. Values are reported in Figure S9 of the supplemental material. PSer is also characterised by a rather high flexibility in the system A_w/Ca/PSer where the phosphate group of the substrate is facing the metal ion. Contrarily, when the carboxylate group is close to the metal ion, i.e., in A/Ca/PSer and A_c/Mg/PSer, the ligand is characterised by a low flexibility. In the case of A_{cw}/Mg/PSer, the phosphate group of the ligand is close to the cavity ion. PSer is constrained and leads to a deformation of the cavity lid as further described in Section B.5. In the system B/Ca/PSer, the bridged binding mode of PSer is a very persistent one, which allows little flexibility of the substrate and results in the high correlation time value of 44 ps. Consequently, the Hbonds occurring between PSer and the enzyme are very stable (Figure S10, supplemental material). The variety of coordination shells and ligand orientations illustrates the great trend of the cavity to accommodate different ions and binding modes.

B.4. Substrate-enzyme interactions

On an energy point of view, the SR cation-PSer interaction energy is very low, below -10^3 kJ/mol, for two magnesium-based systems, i.e., A_{cw}/Mg/PSer and B/Mg/PSer (Table S8, supplemental material). Thus, for those two systems, the strongly negative SR cation-PSer energy largely compensates the repulsive SR hPSP-PSer interaction which originates from the electrostatic interactions with Asp20, Asp179, and Asp183 (Table 3). The number of stabilising PSer-hPSP Hbonds is too low to counterbalance the repulsive character of the negatively charged side chain of the aspartate residues (Table 2). In all simulations, the PSer-Asp22 SR interaction energy is weak, or even negative in the presence of a Hbond, as for A/Ca/PSer and B/Ca/PSer, with values of -21.10 ± 37.81 and -46.94 ± 4.11 kJ/mol, respectively (Table 3).

In each of the simulations, PSer forms Hbonds with a number of water molecules (Table 2). The number of Hbonds formed with the enzyme is lower, below 6, except in the case of the system A_c/Mg/PSer where it exceeds the number of Hbonds it forms with water molecules. In complexes built with the chain B, the number of PSer-hPSP Hbonds is limited compared to chain A-based complexes, and the carboxylate group of the substrate is not involved in Hbonds in the bridged orientation (Table S9, supplemental information).

Table 3. Mean SR PSer-AA interaction energy and standard deviation (kJ/mol) as obtained from the last 100 ns of MD simulations at 300 K and 1 bar.

	PSer-Asp20	PSer-Asp22	PSer-Asp179	PSer-Asp183
A/Ca/PSer	22.59 ± 9.23	-21.10 ± 37.81	16.35 ± 50.26	55.78 ± 9.49
A_w/Ca/PSer	52.65 ± 3.58	27.56 ± 0.21	56.97 ± 28.94	91.74 ± 14.94
A_c/Mg/PSer	53.06 ± 3.26	17.83 ± 14.91	56.59 ± 6.91	104.40 ± 10.55
A_{cw}/Mg/PSer	173.89 ± 32.91	6.42 ± 0.41	150.84 ± 2.89	182.76 ± 28.45
A/Mg/PSer	39.16 ± 1.46	7.52 ± 4.22	23.43 ± 1.80	43.32 ± 1.32
B/Ca/PSer	82.32 ± 16.84	-46.94 ± 4.11	88.35 ± 0.47	99.31 ± 10.72
B/Mg/PSer	180.52 ± 3.98	6.66 ± 2.68	153.30 ± 6.58	179.76 ± 13.44

The positively-charged NH_3 group of PSer (NH3) is always forming Hbonds with Gly29, except in the system B/Mg/PSer wherein they infrequently occur. Lys158, which is close to PSer both in the crystal Chain A and in the artificially built PSer-Chain B complex (Figures 9 and S1), stays always involved in Hbonds with the substrate, either with the phosphate or the carboxylate groups, depending upon its orientation. Thus, whatever the orientation of PSer, it is stabilised in a network of Hbonds within the catalytic site to various extents (Table 2). Such networks are rather stable with time, except for the systems A_w/Ca/PSer, A_c/Mg/PSer, and A_{cw}/Mg/PSer (Figure 10).

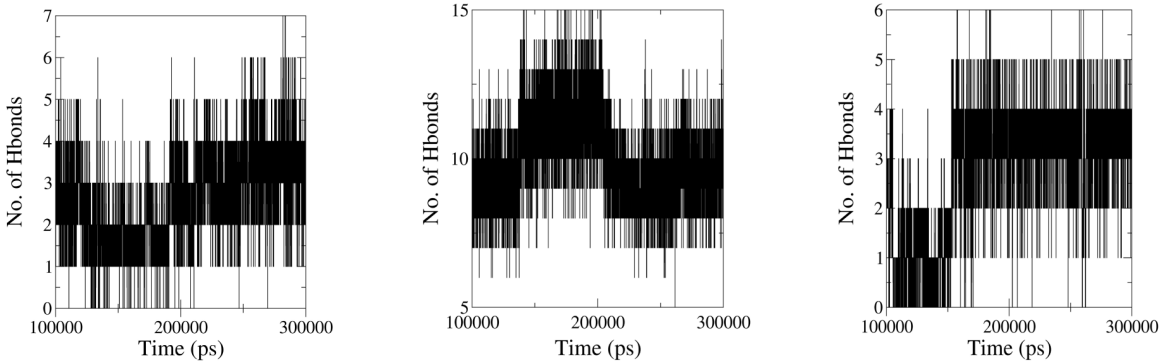

A_w/Ca/PSer A_c/Mg/PSer A_{cw}/Mg/PSer

Figure 10. Number of PSer-hPSP Hbonds as obtained from the last 200 ns of MD simulations at 300 K and 1 bar.

In A_w/Ca/PSer, a drastic loss in the number of PSer-hPSP Hbonds is observed between 130 and 190 ns, corresponding to intermediate states before PSer presents its NH3 close to Glu29. Contrarily, in A_c/Mg/PSer, there is an increase in the number of Hbonds, which occurs between 140 and 210 ns, and is again due to a change in the position of the NH3 group of PSer to eventually form Hbonds with Glu29. For the system A_{cw}/Mg/PSer, the reduced number of Hbonds occurring from 100 to 150 ns involves O-Gly53 Hbonds. Later, both carboxylate O atoms of PSer are Hbonded to the side chain of Arg49. In conclusion, while the orientation of PSer is determined by the interaction of its negatively-charged group with the cation, PSer remains conformationally flexible and rearranges to form NH3-Glu29 Hbonds.

Among stabilisation elements of PSer through electrostatic interactions with the cation and Hbond interactions, arginine residues play an essential role (Table S9, supplemental material). While one side of the active site is paved with several aspartate residues, the other side involves several arginine residues, i.e., Arg49, Arg50, and Arg65 (Figure 1b). They complement Arg202 that faces the lid extremity. Specific interactions between PSer and arginine residues explain the PSer-hPSP SR energy profiles. Particularly, in A_{cw}/Mg/PSer, a decrease from 270 to 110 kJ/mol is observed around t = 147 ns, which corresponds to a flip of Arg49 towards the carboxylate group of PSer (Figure 11a). A second system showing an energy transition due to a particular arginine behaviour is A_c/Mg/PSer wherein Arg50 is involved at t = 135 ns. That specific orientation is actually characterised by several Hbonds that simultaneously involve Arg50, Arg65, and Arg202, i.e., residues located at both sides of the enzyme aperture. The PSer-hPSP interaction energy is the lowest, with a mean value of -615.48 kJ/mol (Table S8, supplemental material). PSer thus acts as a molecule that consolidates the closed form of the enzyme (Section B.5). Around t = 210 ns, Hbonds between NH3 of PSer and Asp179 are lost due to a conformational change in PSer (Figure 11b). Finally, at about 262 ns, PSer comes closer to Lys158. The carboxylate group changes from a position where both carboxyl O atoms interact with the cation to a situation where the carboxylate is shared between Lys158 and Mg^{++} (Figure 11b). Arg50 is also involved in the stabilisation of the B/Ca/PSer system. The low energy conformation observed at t = 213.16 ns is not long-lasting; its energy increases when Arg50 is slightly displaced away from PSer (Figure 11c).

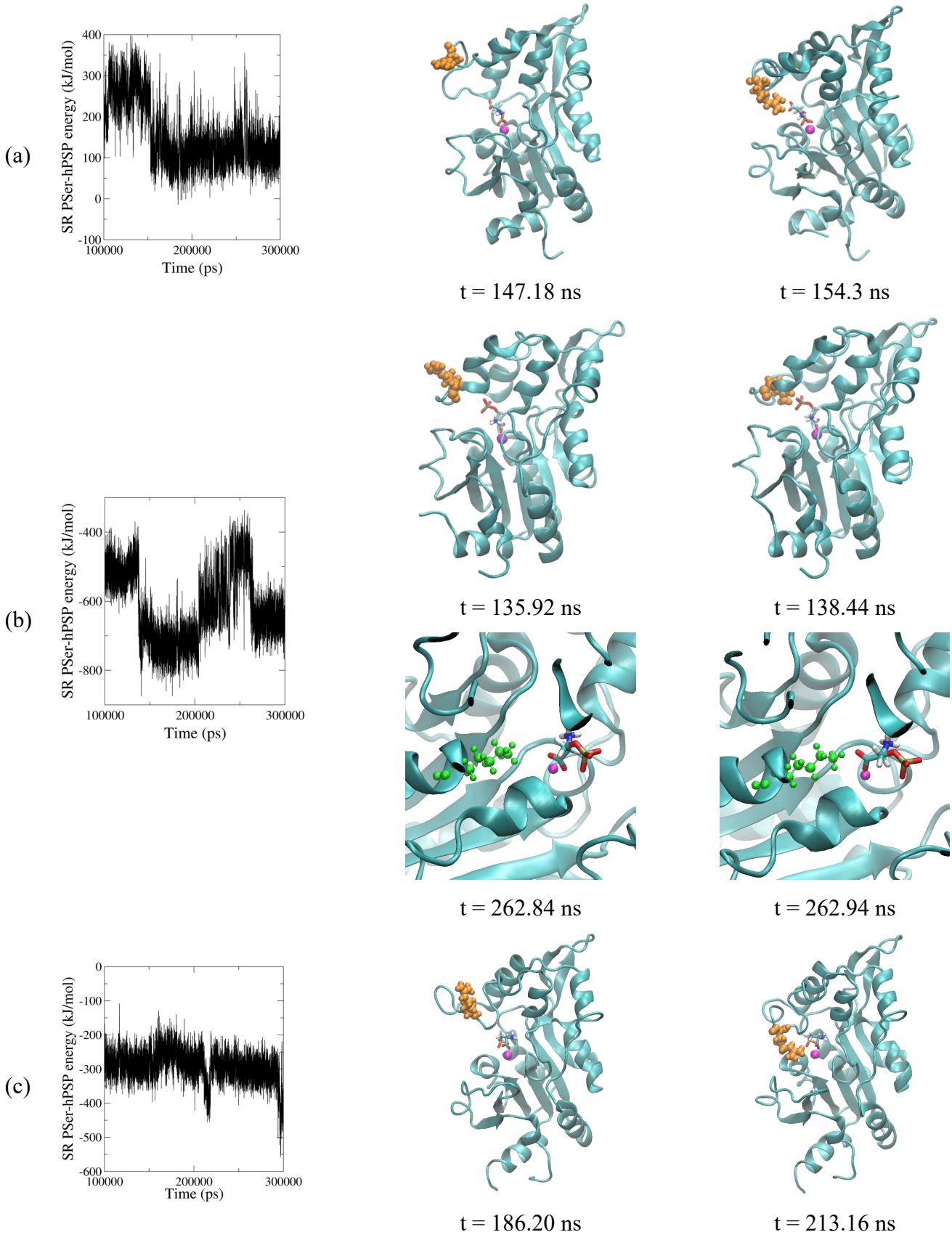

Figure 11. Short-range PSer-hPSP interaction energy profile and snapshots of the systems (a) A_{wc}/Mg/PSer, (b) A_c/Mg/PSer, and (c) B/Ca/PSer, obtained from the last 200 ns of MD simulations at 300 K and 1 bar. Arginine (orange), Lys158 (green), magnesium (magenta).

The hereabove description of the Hbond and electrostatic interactions was completed by an investigation of the non-covalent bond CPs. The present applications mainly focus on the analysis of the intermolecular PSer-hPSP saddle points or passes, i.e., points located below 0.3 nm from the PSer structure. Figure 12 illustrates the intermolecular passes that are detected in the ED of the optimised conformation of the crystal structure of the Ca^{++}-containing PSer-hPSP complex (Table S10, supplemental material).

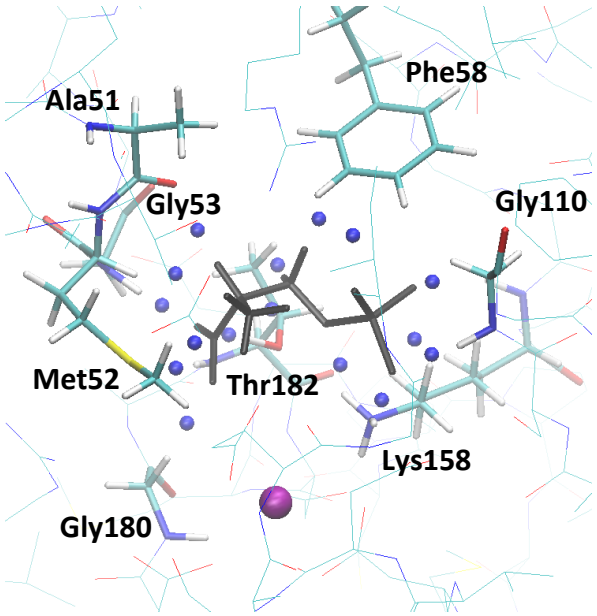

Figure 12. Optimised crystal structure of the chain A of hPSP (lines), Pser (black sticks), Ca^{++} (magenta sphere). The passes (blue spheres) are located at distances ≤ 0.3 nm from PSer. The hPSP residues in interaction with PSer through a pass are shown with sticks.

Selected interaction types are illustrated in Figure 13, e.g., Hbonds with water molecules, a salt bridge identified using the web server PLIP (Salentin et al., 2015), and a phosphate-ion interaction. The list of intermolecular passes and their descriptors are given in Table S10 of the supplemental material. Regarding the optimised crystal structure, 12 weak bonding interactions are detected besides the four Hbonds and strong electrostatic interactions. No passes are found with charged residues such as aspartates, glutamates, and arginines, nor with the cation. Only Lys158 interacts with PSer. Contrarily, the other orientations obtained by MD show different interaction patterns, with strong interactions with the charged residues and the metal cation.

For all systems, many passes are interpreted as bonding NCI in the frame of the Cromer-Mann based ED definition. A number of them are characterised by low ED values, below 0.012 e/bohr^3, while most of the higher ED passes are identified as Hbonds and salt bridges, using tools like the graphics program VMD (Humphrey et al.,1996) and the web server PLIP (Salentin et al., 2015).

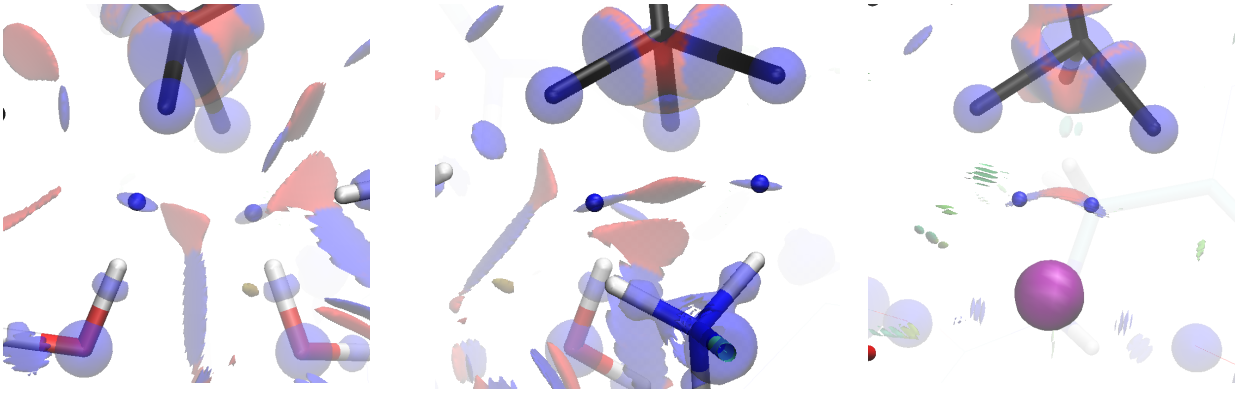

Hbond
PSer(phosphate)-H_2O
A/Mg/PSer

Salt bridge
PSer(phosphate)-Lys158
A/Mg/PSer

PSer(phosphate)-Ion
A_w/Ca/PSer

Figure 13. PSer (black sticks) and selected passes (blue spheres) superimposed to the 0.3 (units = $e^{-1/3}$) isocontour of the RDG (negative (blue) and positive (red) transparent isosurfaces). Similar illustrations with pales (when present) are shown in Figure S11 of the supplemental material.

An analysis of the ED magnitude at the pass locations is achieved to determine whether some orientations can be seen as more stable than the others. For this purpose, a plot of the pass ED magnitude versus the SR interaction energy between PSer and their corresponding hPSP residue is displayed in Figure S12 of the supplemental material. Figure S12 allows to distinguish two areas separating most of the Hbonds and strong electrostatic interactions from the majority of the weaker interactions. The extremely low SR interaction energies, below -10^3 kJ/mol, are associated with phosphate-Mg^{++} interactions, such as in the systems A_{cw}/Mg/PSer and B/Mg/PSer (Table S10). They are also described by highly negative e2 values. A discriminating limit between strong and weak NCI is placed at $\rho = 0.012$ e/bohr^3, which appears to separate PSer-residue interaction energy values below or beyond -30 kJ/mol (Figure S12).

The strong interactions initially observed in the optimised crystal structure are displaced towards the metal cation during all MD simulations. In all cases, Lys158 is systematically involved in strong interactions with PSer, consistently with the observation of the Hbonds presented above, except for the system A/Ca/PSer where NZ of Lys158 is located at a distance of 0.496 nm from OXT of PSer (Table S10). As Lys158 is reported to be involved in the reaction mechanism of the L-serine synthesis, it suggests that the residue is likely well-placed to interact with the substrate, and possibly with the reaction products, in many molecular orientations. Arg49 is involved only in three systems, each time in a strong interaction, and the ion is always involved in NCIs, mostly strong ones, except in the initial crystal structure and when Mg^{++} is screened by water molecules (A/Mg/PSer). Thr182, identified as a key residue by Haufroid et al. (Haufroid et al., 2019) is also always involved in NCIs. Depending upon

the orientation of PSer, the other residues can be involved in strong or weak interactions (Table S10, supplemental material).

On the whole, four intermolecular Hbonds that are identified with VMD are not detected as CPs, but are visualised using contours of the function ***s(r)***. They mostly involve the NH3 group of PSer which interacts with Asp22 or Glu29 (Table S10, supplemental material). It has been reported that weak Hbonds can be identified as NCIs but are not characterised by a ***s(r)*** value of zero (Lane et al., 2013). The precise location of such interaction sites could be approximated by the surrounding ***s(r)*** grid points but it remains largely dependent on the grid size used to visualise the RDG function.

Despite the calculation time required to refine all CPs in the ED distribution functions, the advantage of using a topology-based of the promolecular ED, resides in the single need of molecular geometries to detect Hbonds and other interactions (besides the ED function parameters). The presence of passes is a more direct approach to identify bonding interactions than the consideration of atom-atom distances or the visualisation of ***s(r)*** maps.

B.5. Enzyme open/closed conformations

In a previous paper, Haufroid et al. pointed out the deconstruction of the loop 40-56 between the closed and open conformation of hPSP (Haufroid et al., 2019). In the crystal structure of the chain A of the enzyme, the loop partly involves an α-helix, built on residues 40 to 49. It also involves Met52, located at the helix extremity, close to Ala181 and to the side chain of Arg202. At the level of the lid hinge, the residue Ala35 is Hbonded to Val40. Similarly, in all MD simulations, a Hbond systematically exists between those two residues, regardless of the starting conformations of hPSP. Its breaking can thus hardly be considered as a discriminating descriptor for the opening of the hPSP cavity.

The analysis of the first PC suggests that the open/closed conformation descriptor involves residues located at the tip of the enzyme lid (Figure 6). In the crystal structure of chains A and B, the distance Cα52-Cα202 is equal to 1.00 and 2.25 nm, respectively. The analysis of the MD-based Cα52-Cα202 distance profiles leads to the conclusion that open conformations are rather infrequent and/or not long-living (Figure S13, supplemental material). The longest distances, between 2 and 3 nm, occur in the systems A/Ca/PSer, B/Mg, and B/Ca/PSer. In the chain A-based simulations, large fluctuations appear for the systems containing a calcium ion. Particularly, in A/Ca/PSer, the distance reduces to values around 1 nm at about t = 250 ns. Similarly, in A/Mg/PSer, a definite closure occurs around 210 ns. Low values of the Cα52-Cα202 distance actually reflect the presence of one or several Hbonds formed between amino acid residues of the short sequences 51 to 52 and 202 to 204. A clear example occurs

for the system A/Mg/PSer where a persistent Hbond formed between Met52 and Gln204 leads to very short distance values (Table S11 and Figure S14, supplemental material). That particular Hbond type is also observed in other simulations, especially but not systematically, in the presence of the substrate (Table S11, supplemental material).

For the systems with the most stable Cα52-Cα202 distance profiles, i.e., A_w/Ca/PSer, A_c/Mg/PSer, A_c/Mg, B/Ca/PSer, and B/Mg/PSer, the correlation degree κ_{ij} with the first PC is not very pronounced (Table 1). It is equal to -0.13, 0.40, 0.21, -0.42, and -0.08, respectively. The other simulations yield a view on the closing/opening of the enzyme before definite stabilisation. In the system A_{cw}/Mg/PSer, an increase of the Cα52-Cα202 distance is observed around 158 ns. However, it does not reflect an opening of the enzyme, but rather a deformation of the lid. It is due to the formation of a short π-helix loop involving a Hbond between the C=O group of Met 47 and the N-H group of Met52 (Figure 14). Thus, the distance Cα52-Cα202 can describe conformational changes other than open/closed transitions. It depicts the fluctuations of the lid extremity but does not reflect the overall motion of the lid.

The MD trajectories have also been characterised through a study of the Hbonds formed between the segment Val40 to Val56 of the lid and the helix 29 to 38 of the hPSP core. Figure S15 of the supplemental material reports the minimal distance profiles calculated between the CZ atoms of Arg49 and Arg50 with Glu29. Two main patterns are observed, i.e., values approaching 1.5 nm and distances as short as 0.5 nm or lower. For the complexes built on chain B, it is interesting to note that the distance is shorter when PSer is bound, suggesting that PSer contributes to the closure of the enzyme. Together with Cα52-Cα202 distance profiles, one thus concludes that A/Ca/PSer, A_{cw}/Mg/PSer, and A/Mg/PSer show a closure of the enzyme during the 200 ns MD simulations, while A_c/Mg/PSer and A_c/Mg are definitely closed. On the whole, most of the MD simulations lead to a closed conformation of the hPSP enzyme. System B/Mg/PSer tends to be open, while simulations A_{cw}/Mg/PSer and A/Mg/PSer present a transition from an open-type to a closed form during the final 200 ns of the MD trajectory.

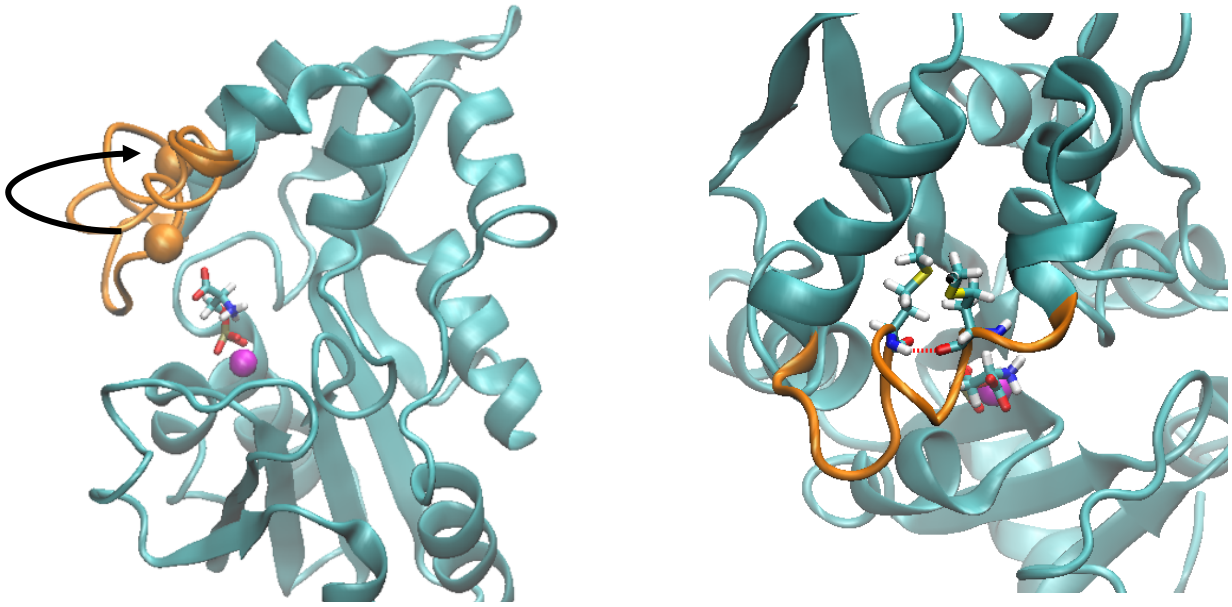

(a) (b)

Figure 14. (a) Structural modification of the enzyme lid in A_{cw}/Mg/PSer observed between t = 100 and 300 ns as obtained from the last 200 ns of the MD simulation at 300 K and 1 bar. Residues 46 to 58 (orange), Cα of Met52 (orange sphere). (b) Details of the Met47-Met52 hydrogen bond (red dashes) at t = 300 ns. Loop 46 to 58 is in orange.

Conclusions

A selected number of human phosphoserine phosphatase (hPSP) complexes are studied using Elastic Network Models (ENM) and Molecular Dynamics (MD) to probe its experimentally observed open and closed conformations as a function of the metal cation type and the presence of the phosphoserine (PSer) substrate. Two metal cation types are considered, either Ca^{++} or Mg^{++}. From crystal structures of the enzyme, the ENM results show that a transition between open and closed states can be explained using a simple protein description and interaction potentials. The complete transition from the open to the closed conformations is more likely to be observed than the inverse transition due to less numerous interactions of the enzyme lid. Principal component analyses (PCA) of the MD trajectories bring details to the ENM results due to the influence of specific interactions. All calcium-dependent systems have a higher first PC eigenvalue than their corresponding magnesium-based system. Their slowest motion is thus characterised by a larger magnitude.

Through MD simulations, several families of substrate orientation inside the enzyme cavity are highlighted, i.e., either the carboxylate, or the phosphate, or both atom groups are oriented towards the metal cation. The latter is observed with Ca^{++}. Sites that are permanently occupied by water molecules are detected around the metal cation where they modulate the interactions with PSer. Two water sites are also observed in the neighbourhood of the lid closure point, as well as a third site shaped like a

small pocket by the surrounding residues. All those water sites are observed in the closed and open crystal structures of the enzyme. The various ligand orientations determine the content of the cation coordination shell and the mobility of the substrate. The weaker the PSer-cation electrostatic interactions, e.g., in the presence of screening water molecules, or when the carboxylate group of PSer directly faces the cation, the higher the flexibility of the substrate. While flexibility of the substrate backbone is observed, energy barriers within the enzyme cavity are large enough to prevent orientation exchanges for the simulation times considered in the present work. The orientation of PSer is determined by the interaction of its negatively charged groups with the cation. PSer remains conformationally flexible, except when bridged, and rearranges to form NH3-Glu29 Hbonds. Using various MD starting points is thus a way to probe possible ligand positions.

The MD analyses suggest that the possibility for the substrate to adopt several orientations in the presence of Ca^{++} might be a statistical and geometrical reason for the lower activity of the calcium-dependent form of the enzyme. Even in the presence of Mg^{++}, various orientations are observed and are likely not all efficient for the occurrence of the enzyme reaction. Additionally, PSer is closer to the magnesium ion than it is to the calcium ion. Finally, the coordinated oxygen atoms are drastically less mobile when bound to Mg^{++}. The variety of coordination shells and ligand orientations illustrates the great trend of the cavity to accommodate different ions and binding modes.

A global description of the strong (Hbonds and strong electrostatics) and weak interactions occurring between the substrate and the enzyme was obtained using a critical point analysis of the Cromer-Mann based promolecular electron density (ED) distribution function. Passes (saddle points) of the ED are used as locators of the non-covalent interactions, which are distinguished using their ED magnitude. The approach was applied to the last frame of each simulation and showed that two hPSP residues known to be involved in the enzyme reaction mechanism, Lys158 and Thr182, are systematically interacting with the substrate.

Specific intra-enzyme and hPSP-PSer interactions are observed depending on the conformation of the enzyme and the orientation of the substrate. Preferably closed enzyme conformations are distinguished from specific interactions, e.g., the Met52-Gln204 interaction that involves the lid extremity and its facing residues. The closed state can also be consolidated when the substrate simultaneously interacts with both sides of the enzyme aperture, through Hbonds with several arginine residues. Arg49-Glu29 and Arg50-Glu29 interactions also confirm the enzyme closure state. In parallel, Met52, Arg49, and Arg50 are also involved in the stabilisation of PSer inside the binding site of hPSP. More open conformations most often occur when the phosphate group is close the enzyme lid, or in the absence of the substrate.

Considering the low mobility of PSer inside the cavity, it is an interesting prospect to determine whether the way the substrate enters the cavity is decisive in its reactivity likeliness. Techniques like steered MD or umbrella sampling might be used. The unclear point would be to determine plausible initial and final complexation states between the substrate and the ligand.

Modifications brought to the alternating pattern of oppositely-charged elements, i.e., positive lid - negative substrate – position metal ion – negative cavity surface, are considered. A systematic search of databases could help in determining such kind of patterns. In the present work, only modification of the metal ion type has been considered on a purely classical approach. Other types of changes can be proposed, such as the modification of the protonation state of the cavity and the lid residues, especially the aspartate and arginine residues, respectively. Tools such as PROPKA (Davies et al., 2006) can be used to focus on residues that are likely to adopt several protonation states, while on a more prospective basis, mutations could be tested (Collet et al. 1999, Veiga da Cunha et al. 2004).

In its current status, the search for the CPs is applied to single MD frames. An interesting aspect would be to extent such a kind of analysis to MD trajectories so as to generate the so-called Spatial Distribution Functions to give access to the three-dimensional occurrence distribution of the PCs and the corresponding interactions (Svishchev & Kusalik, 1993; Kulińska et al., 2000).

Acknowledgments

Frédéric Wautelet and Laurent Demelenne are gratefully acknowledged for program installation and maintenance. This research used resources of the ‘Plateforme Technologique de Calcul Intensif (PTCI)’ (http://www.ptci.unamur.be) located at the University of Namur, Belgium, which is supported by the FNRS-FRFC, the Walloon Region, and the University of Namur (Conventions No. 2.5020.11, GEQ U.G006.15, 1610468 et RW/GEQ2016). The PTCI is member of the ‘Consortium des Équipements de Calcul Intensif (CÉCI)’ (http://www.ceci-hpc.be), funded by the ‘Fonds de la Recherche Scientifique de Belgique (F.R.S.-FNRS)’ under the Grant No. 2.5020.11 and by the Walloon Region.

References

Bader R. F. (2001). The zero-flux surface and the topological and quantum definitions of an atom in a molecule. *Theoretical Chemistry Accounts*, *105*(4-5),276-283.

Baron R., van Gunsteren W. F. & Hünenberger Ph. (2006). Estimating the configurational entropy from Molecular Dynamics simulations: Anharmonicity and correlation corrections to the quasi-harmonic approximation. *Trends in Physical Chemistry*, *11*,87-122.

Boto R. A., Contreras-García J., Tierny J. & Piquemal J. -P. (2015). Interpretation of the reduced density gradient. *Molecular Physics*, *114*(7-8),1406-1414.

Brassier A., Valayannopoulos V., Bahi-Buisson N., Wiame E., Hubert L., Boddaert N., Kaminska A., Habarou F., Desguerre I., Van Schaftingen E., Ottolenghi C. & de Lonlay P. (2016). Two new cases of serine deficiency disorders treated with L-serine. *European Journal of Paediatric Neurology*, *20*(1),53-60.

Collet J.-F., Gerin I., Rider M. H., Veiga da Cunha M. & Van Schaftingen E. (1997). Human L-3-phosphoserine phosphatase: Sequence, expression and evidence for a phosphoenzyme intermediate. *FEBS Letters*, *408*(3),281-284.

Collet J.-F., Stroobant V. & Van Schaftingen E. (1999). Mechanistic studies of phosphoserine phosphatase, an enzyme related to P-type ATPases. *Journal of Biological Chemistry*, *274*(48), 33985-33990.

Davies M. N., Toseland Ch. P., Moss D. S. & Flower D. R. (2006). Benchmarking pKa prediction, BMC Biochemistry, *7*,18.

de Koning T. & Klomp L. (2004) Serine-deficiency syndromes. *Current Opinion in Neurology*, *17*(2),197-204.

DeBerardinis R. J. (2011). Serine metabolism: Some tumors take the road less traveled. *Cell Metabolism*, *14*(3), 285-286.

Gironés X., Carbó-Dorca R. & Mezey P. G. (2001). Application of promolecular ASA densities to graphical representation of density functions of macromolecular systems. *Journal of Molecular Graphics Modelling*, *19*(3-4),343-348.

Haufroid M., Mirgaux M., Leherte L. & Wouters J. (2019). Crystal structures and snapshots along the reaction pathway of human phosphoserine phosphatase. *Acta Crystallographica D*, *75*,592-604.

Hess B., Kutzner C., van der Spoel D. & Lindahl E. (2008). GROMACS 4: Algorithms for highly efficient, load-balanced, and scalable molecular simulation. *Journal of Chemical Theory and Computation*, *4*(3),435-447.

Humphrey W., Dalke A. & Schulten K. (1996). VMD - Visual Molecular Dynamics. *Journal of Molecular Graphics*, *14*(1),33-38.

Ibers J. A. & Hamilton W. C. (Eds). (1974). *International tables for X-ray crystallography*, Vol. IV. Kynoch Press, Birmingham.

Jaeken J. (2012). Disorders of proline and serine metabolism. In: Saudubray J. M., van den Berghe G. & Walter J. H. (Eds.) *Inborn metabolic diseases*. Springer, Berlin,357-362.

Jiao D., King Ch., Grossfield A., Darden Th. A. & Ren P. (2006). Simulation of Ca2+ and Mg2+ solvation using polarizable atomic multipole potential. *The Journal of Physical Chemistry B*, *110*(37),18553-18559.

Jing Z., Liu C., Qi R. & Ren P. (2018). Many-body effect determines the selectivity for Ca^{2+} and Mg^{2+} in proteins. *Proceedings of the National Academy of Sciences of the United States of America*, *115*(32),E7495-E7501.

Johnson E. R., Keinan S., Mori-Sánchez P., Contreras-García, Cohen A. J. & Yang W. (2010). Revealing Noncovalent Interactions. *The Journal of the American Chemical Society*, *132*(18),6498-6506.

Kulińska K., Kuliński T., Lyubartsev A., Laaksonen A. & Adamiak R. W. (2000). Spatial distribution functions as a tool in the analysis of ribonucleic acids hydration - molecular dynamics studies. *Computers & Chemistry*, *24*(3-4),451-457.

Lane J. R., Contreras-García J., Piquemal J. -Ph., Miller B. J. & Kjaergaard H. G. (2013). Are bond critical points really critical for hydrogen bonding? *Journal of Chemical Theory and Computation*, *9*(8),3263-3266.

Leherte L. (2004). Hierarchical description of protein structure fragments obtained from analyses of promolecular electron density distributions. *Acta Crystallographica A*, 60,1254-1265.

Li X., Xun Z. &Yang Y. (2016). Inhibition of phosphoserine phosphatase enhances the anticancer efficacy of 5-fluorouracil in colorectal cancer. *Biochemical and Biophysical Research Communications*, *477*(4),633-639.

Lindorff-Larsen K., Piana S., Palmo K., Maragakis P., Klepeis J. L., Dror R. O. & Shaw D. E. (2010). Improved side-chain torsion potentials for the Amber ff99SB protein force field. *Proteins*, *78*(8),1950-1958.

López-Blanco J. R., Aliaga J. I., Quintana-Ortí E. S. & Chacón P. (2014) iMODS: Internal coordinates normal mode analysis server. *Nucleic Acids Research*, *42*,W271-276. (http://imods.chaconlab.org/, last accessed 22 Sept. 2019).

Mullarky E., Lucki N. C., Zavareh, R. B.; Anglin J. L., Gomes, A. P.; Nicolay B. N., Wong J. C. Y., Christen S., Takahashi H., Singh P. K., Benis J., Warren J. D., Fendt S.-M., Asara J. M., DeNicola G. M., Lyssiotis C. A., Lairson L. L. & Cantley L. C. (2016). Identification of a small molecule inhibitor of 3-phosphoglycerate dehydrogenase to target serine biosynthesis in cancers. *Proceedings of the National Academy of Sciences*, *113*(7),1778-1783.

Orellana L., Rueda M., Ferrer-Costa C., Lopez-Blanco J. R., Chacón P. & Orozco M. (2010). Approaching elastic network models to Molecular Dynamics flexibility. *Journal of Chemical Theory and Computation*, *6*(9),2910-2923.

Peeraer Y., Rabijns A., Verboven C., Collet J.-F., Van Schaftingen E. & De Ranter C. (2002). Purification, crystallization and preliminary X-ray diffraction analysis of human phosphoserine phosphatase. *Acta Crystallographica D*, *58*,133-134.

Peeraer Y., Rabijns A., Verboven Ch., Collet J.-F., Van Schaftingen E. & De Ranter C. (2003). High-resolution structure of human phosphoserine phosphatase in open conformation, *Acta Crystallographica D*, *59*,971-977.

Peeraer Y., Rabijns A., Collet J.-F., Van Schaftingen E. & De Ranter C. (2004). How calcium inhibits the magnesium-dependent enzyme human phosphoserine phosphatase. *European Journal of Biochemistry*, *271*(16),3421-3427.

Piovesan D., Minervini G. & Tosatto S. C. E. (2016). The RING 2.0 web server for high quality residue interaction networks. *Nucleic Acids Research*, *44*,W367-374.

Pronk S., Páll S., Schulz R., Larsson P., Bjelkmar P., Apostolov R., Shirts M. R., Smith J. C., Kasson P. M., van der Spoel D., Hess B. & Lindahl E. (2013). GROMACS 4.5: A high-throughput and highly parallel open source molecular simulation toolkit. *Bioinformatics*, *29*(7),845-854.

Salentin S., Schreiber S., Haupt V. J., Adasme M. F. & Schroeder M. (2015). PLIP: fully automated protein–ligand interaction profiler. *Nucleic Acids Research*, *43*(W1),W443-W447.

Sato K., Masuda T., Hu Q., Tobo T., Kidogami S., Ogawa Y., Saito T., Nambara S., Komatsu H., Hirata H., Sakimura S., Uchi R., Hayashi N., Iguchi T., Eguchi H., Ito S., Nakagawa T. & Mimori K. (2017). Phosphoserine Phosphatase Is a Novel Prognostic Biomarker on Chromosome 7 in Colorectal Cancer. *Anticancer Research*,*37*(5),2365-2371.

Svishchev I. M. & Kusalik P. G. (1993). Structure in liquid water: A study of spatial distribution functions. *Journal of Chemical Physics*, 99(4), 3049-3058.

Tabatabaie L., Klomp L. W., Berger R. & de Koning T. J. (2010). L-serine synthesis in the central nervous system: A review on serine deficiency disorders. Molecular Genetics and Metabolism, *99*(3),256-262.

Veiga da Cunha M., Collet J.-F., Prieur B., Jaeken J., Peeraer Y., Rabbijns A. & Van Schaftingen E. (2004). Mutations responsible for 3-phosphoserine phosphatase deficiency, *European Journal of Human Genetics*, *12(*2),163-166.

Wang X., Kirberger M., Qiu F., Chen G. & Yang J. J. (2008). Towards predicting Ca2+-binding sites with different coordination numbers in proteins with atomic resolution, *Proteins*, *75*(4),787-798.

Yoon S., Kim J. G., Seo A. N., Park S. Y., Kim H. J., Park J. S., Choi G. S., Jeong J. Y., Yoon G. S., Kang B. W. (2015). Clinical implication of serine metabolism-associated enzymes in colon cancer. *Oncology*, *89*(6),351-359.

Supplemental online material

Investigation of bound and unbound phosphoserine phosphatase conformations through Elastic Network Models and Molecular Dynamics simulations

Laurence Leherte, Marie Haufroid, Manon Mirgaux, Johan Wouters

Laboratoire de Chimie Biologique Structurale, Unité de Chimie Physique Théorique et Structurale, Department of Chemistry, NAmur Research Institute for LIfe Sciences (NARILIS), NAmur MEdicine & Drug Innovation Center (NAMEDIC), Namur Institute of Structured Matter (NISM), University of Namur, Rue de Bruxelles 61, B-5000 Namur (Belgium)

S1. Ligand and enzyme structure building

Starting from the crystal structure coordinates of phosphoserine (PSer), hydrogen atoms were added with VegaZZ (Pedretti et al., 2004). The resulting structure was then grossly optimised using the steepest descent algorithm of VegaZZ with a tolerance of 1.0 $kcal.mol^{-1}.Å^{-1}$, a high value selected to prevent any drastic modification of the heavy atoms coordinates. Gromacs coordinates and topology files were generated using Topolbuild (Ray, 2009). Parameters reported in references (Homeyer et al., 2006; Steinbrecher et al., 2012) were considered so as to retain a conformational degeneracy of the three phosphate oxygen atoms. All three P-O distances were kept identical.

The atomic charges of PSer were determined using the Quantum Mechanics program Gaussian (Frisch et al., 2009) at the RHF/6-31G(d) level, a molecular electrostatic potential (MEP) grid of 250 x 250 x 250 elements and a grid interval of 0.1 Å was generated according to the Merz-Singh-Kollman scheme (Singh & Kollman, 1984; Besler et al., 1990). A modified version of QFIT (Borodin & Smith, 2009) was run to determine the atomic charges (Table S1). The program code was adapted so as to fit electrostatic forces calculated from electrostatic potential grids, as described in Ref. (Leherte, 2016).

Table S1. RHF/6-31G(d) atomic charges ($|e^-|$) of PSer obtained using Gaussian (Frisch et al., 2009).

Atom	Net charge	Atom	Net charge
N	-0.8460	CB	0.0728
H1, H2, H3	0.4196	HB1, HB2	0.0471
CA	0.1600	OG	-0.5204
HA	0.0178	OXT	-0.8163
C	0.8860	O1P, O2P, O3P	-0.9962
O	-0.8163	P	1.4980

From the reference MEP grids, fittings were achieved by considering points located at distances between 1.4 and 2.0 times the van der Waals radius of the atoms. These two limiting distance values were selected after the so-called Merz-Singh-Kollman scheme (Singh & Kollman, 1984). Constraints, such as the total molecular charge (-2 $|e^-|$) and the total dipole moment were applied. Additional constraints were considered so as to force the atomic charges of the atoms H1, H2, and H3, to be equal, as well as for atoms HB1 and HB2, and O1P, O2P, and O3P.

Regarding the protein, the missing three first amino acid residues of chainA, Met1-Ile2-Ser3, were added using the following procedure. First, chain B, which contains the first three residues, was aligned onto chain A. The residue coordinates were saved and added to the incomplete chain A. The chain B of hPSP-PSer was selected to model the open form of the enzyme. The missing amino acid side chains of residues 47 to 50 were generated using the web server BetaSCPWeb (Ryu et al., 2016). Both enzyme structures were protonated using the standard protonation states of the amino acid residues, i.e., charged end residues, positive Lys and Arg, and negative Glu and Asp.

S2. Molecular Dynamics simulations

MD trajectories of the solvated systems were run using the Gromacs 4.5.5 program package (Hess et al., 2008; Pronk et al., 2013) with the Amber99sb-ildn FF (Lindorff-Larsen et al., 2010) under particle mesh Ewald (PME) periodic boundary conditions and a Coulomb cut-off distance of 1.0 nm. The ligand PSer was described using the Amber Force Field parameters reported in (Homeyer et al., 2006; Steinbrecher et al., 2012). The Newton equations of motion were numerically integrated using a leap-frog integrator. The van der Waals cut-off distance was set equal to 1.2 nm. Long-range dispersion corrections to energy and pressure were applied. The systems were optimised using a steepest descent algorithm with an initial step size of 0.10 nm. To strongly reduce the calculation time, the hybrid TIP3P/SIRAH water FF was used (Darré et al., 2012; Gonzáles et al., 2013; Darré et al., 2015). The initial protein systems (with and without ligand) were solvated so as protein atoms lie at least at a distance of 2.0 nm from the cubic box walls. A shell of 1.0 nm thickness of TIP3P water molecules was defined around the protein complex, and the remaining space of the solvation box was filled with SIRAH water beads (Machado et al., 2018) where each bead is composed of four interaction sites and represents about 11 water molecules. A mix of SIRAH Na^+ and K^+ ions were added to cancel the electric charge of the systems.

Various MD simulations were carried out (Figure 2 and Table S2).

Table S2. Description of the protein systems simulated using Gromacs at T = 300 K, and at P = 1 bar in hybrid TIP3P/SIRAH water.

	Total no. of particles	No. of all-atom/CG water molecules	Total no. of ions	Final box size (nm)
Chain A – based MD				
A/Ca/PSer	25,202	3,372/2,883	3 K^+, 2 Na^+	10.36499
A_w/Ca/PSer	25,556	3,502/2,874	3 K^+, 2 Na^+	10.37705
A/Mg/PSer	25,202	3,372/2,883	3 K^+, 2 Na^+	10.35826
A_c/Mg/PSer	25,202	3,372/2,883	3 K^+, 2 Na^+	10.35826
A_{cw}/Mg/PSer	25,556	3,502/2,874	3 K^+, 2 Na^+	10.36459
A_c/Mg	25,183	3,372/2,883	3 K^+	10.37098
A_{cw}/Mg	25,537	3,502/2,874	3 K^+	10.38672
Chain B – based MD				
B/Ca	26,886	3,709/3,056	3 K^+	10.56515
B/Mg	26,886	3,709/3,056	3 K^+	10.57560
B/Ca/PSer	26,887	3,707/3,053	3 K^+, 2 Na^+	10.56797
B/Mg/PSer	26,887	3,707/3,053	3 K^+, 2 Na^+	10.56653

In simulations A/Ca/PSer and A/Mg/PSer, a calcium (or magnesium) ion was considered at the crystallographic position of Ca^{++} in the active site. Crystallographic water molecules were added in simulation A_w/Ca/PSer to generate a second starting configuration of the system involving PSer and Ca^{++}. Among the crystallographic water, 101 molecules were selected according to their proximity of the PSer/hPSP structures. The final conformations of the systems A/Ca/PSer and A_w/Ca/PSer were used as starting points for the simulations of magnesium-dependent systems, named A_c/Mg/PSer and A_{cw}/Mg/PSer. The last frame of these two simulations were themselves used as starting configurations of substrate-free systems, named A_c/Mg and A_{cw}/Mg, respectively.

Simulations of the open chain B were achieved considering calcium and magnesium metal ions, with and without the substrate PSer.

The whole systems were again optimised to eliminate large forces, using a steepest descent algorithm with an initial step size of 0.10 nm, and then heated to 50 K through a 10 ps canonical (NVT)

MD, with a time step of 2 fs and LINCS constraints acting on bonds involving H atoms. The trajectory was followed by two successive 20 ps heating stages, at 150 K and at the final temperature of 300 K, under the same conditions. Next, each system was equilibrated during 50 ps in the NPT ensemble, at P = 1 bar, to relax the solvent molecules, and for a further 60 ns MD equilibration run. The 'V-Rescale' and 'Parrinello-Rahman' algorithms were selected to constrain T and P, respectively. A final run of 300 ns (150 x 10^6 steps) was performed for the evaluation of the structural, energetics, and dynamical properties of each system. Trajectory data were saved every 20 ps.

Only the last 200 ns of that final run were used as the production stage to eliminate the most fluctuating part of the trajectories. Consequently, the equilibration stage duration is equal to 160 ns.

Table S3. ED parameters $w'_{a,i}$ (no unit) and $\zeta'_{a,i}$ (bohr^{-2}) coefficients as obtained to fit the Cromer-Mann parameters. The mathematical relationships and the parameter values for the atom types C, N, O, and S are given in (Leherte, 2004).

	H	P	Ca^{++}	Mg^{++}
w_1'	0.16854600	0.46415333	0.10788983	0.28236667
ζ_1'	1.56469094	3.03261175	3.75576265	2.63869650
w_2'	0.56040540	0.27319333	0.33417363	0.33042500
ζ_2'	0.46127543	0.20714039	15.7577288	1.18568426
w_3'	0.00537593	0.15659333	0.42716802	0.14668333
ζ_3'	20.2478100	34.0072686	0.53608875	47.8823755
w_4'	0.26525298	0.10598000	0.03239855	0.07385417
ζ_4'	0.16430279	0.08324861	0.21165146	0.55016835

Table S4. First three eigenvalues (nm^2) obtained from the PCA of hPSP as obtained from the last 200 ns of MD trajectories at 300 K and 1 bar.

	λ_1	λ_2	λ_3
Chain A			
A/Ca/PSer	1.110	0.469	0.221
A_w/Ca/PSer	0.925	0.255	0.168
A_c/Mg/PSer	0.783	0.352	0.169
A_{cw}/Mg/PSer	0.652	0.186	0.139
A/Mg/PSer	0.726	0.371	0.095
A_c/Mg	0.415	0.287	0.191
A_{cw}/Mg	0.598	0.267	0.173
Chain B			
B/Ca	0.521	0.322	0.207
B/Mg	0.455	0.275	0.264
B/Ca/PSer	0.855	0.185	0.132
B/Mg/PSer	0.602	0.306	0.197

Table S5. Cation coordination with oxygen atoms as reported from experiments (Peerear et al., 2004; Haufroid et al., 2019) and the last 200 ns of MD simulations at 300 K and 1 bar. A cutoff value of 0.25 and 0.35 nm is used when Mg^{++} and Ca^{++} are considered, respectively. Integration under the first peak of the radial distribution functions g(ion-oxygen) is given in parentheses

Magnesium-dependent hPSP (Peerear et al., 2004) Asp20 (OD1) Asp22 (O) Asp179 (OD2) Three H_2O	*Calcium-dependent hPSP* (Peerear et al., 2004) Asp20 (OD1, OD2) Asp22 (O) Asp179 (OD2) Three H_2O
(Haufroid et al., 2019) Asp20 (OD1, OD2) – 0.311 and 0.225 nm Asp22 (O) – 0.231 nm Asp179 (OD1, OD2) – 0.218 and 0.342 nm Three H_2O – 0.224, 0.242, 0.242 nm	
A/Ca/PSer (8.2) – Figure 7b Asp20 (partly OD1, OD2) Asp22 (O, OD1) Asp179 (OD1) Asp183 (OD1, OD2) PSer (O) Exchangeable H_2O	*A_w/Ca/PSer (8.6)* – Figure 7a Asp20 (OD1, OD2) Asp22 (O) Asp179 (OD1) Asp183 (OD1, OD2) PSer (O1P in a less extent, O2P, O3P)
A_c/Mg/PSer (5.7) Asp20 (OD2) Asp22 (OD2) Asp179 (OD1) Asp183 (OD1, OD2) PSer (O)	*A_{cw}/Mg/PSer (6.0)* Asp20 (OD2) Asp179 (OD1) Asp183 (OD2) PSer (O1P, O2P, O3P)
A/Mg/PSer (6.0) – Figure 7d Asp20 (OD1, OD2) Asp22 (O) Asp179 (OD1) Two permanent water molecules	
A_c/Mg (6.0) Asp20 (OD1, OD2) Asp22 (O, OD2) Asp179 (OD1) Asp183 (OD1)	*A_{cw}/Mg (6.0)* Asp20 (OD2) Asp22 (O) Asp179 (OD1) Asp183 (OD2) Two permanent water molecules
B/Ca (8.9) Asp20 (OD2) Asp22 (O) Asp179 (OD1, OD2) Asp183 (OD1, OD2) Non-permanent water molecules	*B/Mg (6.0)* Asp20 (OD2) Asp22 (O) Asp179 (OD1, OD2) Asp183 (OD2) One permanent water molecule
B/Ca/PSer (8.0) – Figure 7c Asp20 (OD2) Asp179 (OD1) Asp183 (OD1, OD2) PSer (O, O2P, O3P) One permanent water molecule	*B/Mg/PSer (6.0)* Asp20 (OD2) Asp179 (OD1) Asp183 (OD2) PSer (O1P, O2P, O3P)

Table S6. RMSF (nm) of coordinated oxygen atoms (Table S5) as obtained from the last 200 ns of MD simulations at 300 K and 1 bar.

	Total	Asp	PSer	H_2O
A/Ca/PSer	1.51 ± 1.12	0.95 ± 0.07	3.80	/
A_w/Ca/PSer	2.12 ± 0.75	1.59 ± 0.06	1.59 ± 0.06	/
A_c/Mg/PSer	1.35 ± 0.61	0.95 ± 0.02	/	1.82, 2.50
A_{cw}/Mg/PSer	0.11 ± 0.05	0.12 ± 0.06	0.07	/
A/Mg/PSer	0.15 ± 0.04	0.18 ± 0.04	0.12 ± 0.000(9)	/
A_c/Mg	0.03 ± 0.01	0.03 ± 0.01	/	/
A_{cw}/Mg	0.01 ± 0.000(6)	0.01 ± 0.000(8)	/	0.011, 0.011
B/Ca	0.06 ± 0.03	0.06 ± 0.03	/	/
B/Mg	1.11 ± 0.99	0.67 ± 0.05	/	3.31
B/Ca/PSer	2.48 ± 0.10	2.48 ± 0.10	2.46 ± 0.09	2.55
B/Mg/PSer	0.01 ± 0.000(7)	0.01 ± 0.000(2)	0.01 ± 0.000(9)	/

Table S7. Occurrence frequency (> 20 %) and hydrogen bonds formed by of water molecules in contact (d ≤ 0.4 nm) with residues Asp179, Phe196, Gly197, and Val200 to Arg202, as obtained from the last 200 ns of MD trajectories at 300 K and 1 bar.

	Occurrence frequency	Hbonds formed with
A/Ca/PSer	100	Asp179, Val200, Arg202
	100	Phe196, Val200
A_w/Ca/PSer	100	Asp179, Phe196, Val200, Arg202
	98	Phe196, Val200
A_c/Mg/PSer	69	Phe196, Val200
	52[a]	Asp179, Phe196, Val200, Arg202
	41[b]	Asp179, Phe196, Val200, Arg202
	21[c]	Asp179, Phe196, Val200, Arg202[d]
	21[e]	Asp179, Phe196, Val200, Arg202
A_{cw}/Mg/PSer	64	Asp179[f], Phe196[f], Val200[f], Arg202[f]
	64	Phe196[g], Val200[g]
	32	Asp179, Phe196[h], Val200[h], Arg202[h]
A/Mg/PSer	100	Asp179, Val200, Arg202
	76	Phe196, Val200
A_c/Mg	76	Phe196, Val200
	67[i]	Asp179, Phe196, Val200, Arg202
A_{cw}/Mg	81[j]	Asp179, Phe196, Val200, Arg202
	48[k]	Phe196, Val200
	40[l]	Phe196, Val200
B/Ca	97	Phe196, Val200
	93	Asp179, Phe196, Val200, Arg202
	33[m]	Asp179, Phe196, Val200, Arg202
B/Mg	80	Phe196, Val200
B/Ca/PSer	27[n]	Asp179, Phe196
B/Mg/PSer	100	Phe196, Val200
	52[o]	Asp179, Phe196, Val200, Arg202
	28[o]	Asp179, Phe196, Val200, Arg202
	21[o]	Asp179, Phe196, Val200, Arg202

[a] 100-202 ns; [b] 202-300 ns; [c] 166-210 ns; [d] 210-238 ns; [e] 220-271 ns; [f] After 157 ns; [g] After 130 ns; [h] After 205 ns; [i] 100-234 ns; [j] 100 to 262 ns; [k] 100 to 205 ns; [l] from 205 ns; [m] 230-300 ns; [n] 190-300 ns; [o] Three exchanging water molecules at a single site.

Table S8. Mean short-range interaction energy and standard deviation (kJ/mol) as obtained from the last 200 ns of MD simulations at 300 K and 1 bar.

	Cation-H_2O	Cation-PSer	hPSP-PSer
A/Ca/PSer	-21.76 ± 51.76	-190.54 ± 29,80	-381.53 ± 56.94
A_w/Ca/PSer	125.62 ± 45.85	-515.65 ± 62.58	-122.43 ± 68.13
A_c/Mg/PSer	135.54 ± 35.11	-412.73 ± 100.91	-615.48 ± 101.31
A_{cw}/Mg/PSer	274.20 ± 34.62	-1386.35 ± 34.50	155.67 ± 75.93
A/Mg/PSer	-405.29 ± 32.13	-117.97 ± 26.34	-294.65 ± 55.05
A_c/Mg	139.21 ± 82.29	/	/
A_{cw}/Mg	-423.70 ± 34.00	/	/
B/Ca	-272.91 ± 74.55	/	/
B/Mg	-195.07 ± 31.90	/	/
B/Ca/PSer	70.18 ± 30.43	-629.55 ± 26.54	-291.47 ± 43.94
B/Mg/PSer	286.69 ± 34.75	-1389.37 ± 35.59	171.70 ± 57.35

Table S9. Most frequent PSer-hPSP Hbond types as obtained from the last 200 ns of MD simulations at 300 K and 1 bar. The ligand orientation is described using the PSer group in interaction with the metal ion.

	PSer-hPSP Hbond type	Ligand orientation
A/Ca/PSer	nh3-Glu29 po3-Arg65 O-Lys158, Thr182	coo-metal
A_w/Ca/PSer	nh3-Glu29, Asp179 po3-Ser23, Lys158 O-Gly53	po3-metal
A_c/Mg/PSer	nh3-Asp22, Glu29 po3-Arg50, Arg65, Arg202 O-Lys158	coo-metal
A_{cw}/Mg/PSer	nh3-Glu29 po3-Lys158 O-Arg49, Gly53	po3-metal
A/Mg/PSer	nh3-Glu29 po3-Lys158, Thr182 O-Arg202	screened po3-metal
B/Ca/PSer	nh3-Asp22, Glu29 po3-Arg49, Lys158	bridged
B/Mg/PSer	po3-Lys158 O-Thr48, Arg49	po3-metal

Table S10. Intermolecular passes (located at a distance ≤ 0.3 nm from PSer) detected in the optimised crystal structure and in the last frame of the MD trajectories of the PSer-hPSP complexes as obtained from a topological analysis of the Cromer-Mann based promolecular ED distribution function. SR interaction energy value are given for pairs PSer - residue of hPSP. Hbonds and salt bridges (bold) are identified using VMD (Humphrey et al.,1996) and PLIP (Salentin et al., 2015).

PSer atom	hPSP atom	ρ (e/bohr^3)	e2 (e/bohr^5)	Energy (kJ/mol)
Optimised crystal structure				
HA	Ala51(O)	0.0092	-0.0085	-2.27
O2P	**Gly110(H)**	**0.0273**	**-0.0293**	-57.51
O1P	Gly110(HA1)	0.0096	-0.0021	
OXT	Gly180(HA)	0.0021	-0.0014	-16.59
O	**Gly53(H)**	**0.0400**	**-0.0555**	-30.34
O1P	Lys158(HE1)	0.0099	-0.0015	-156.51
O2P	**Lys158(HZ1)**	**0.0232**	**-0.0246**	
OG	Lys158(HZ2)	0.0124	-0.0082	
CA	Met52(S)	0.0085	-0.0024	-17.37
HA	Met52(HA)	0.0090	-0.0055	
OXT	Met52(S)	0.0102	-0.0049	
O3P	Phe58(CE1)	0.0070	-0.0009	-11.60
HB2	Phe58(HE1)	0.0063	-0.0028	
O	**Thr182(HG1)**	**0.0548**	**-0.0813**	-58.53
HB1	Thr182(HG1)	0.0102	-0.0022	
HB1	Thr182(HG21)	0.0114	-0.0091	
A/Ca/PSer				
O	**Arg202(HH21)**	**0.0362**	**-0.0467**	-56.52
O3P	Arg50(HB2)	0.0005	-0.0004	-3.30
HB2	Arg50(O)	0.0003	-0.0002	
O2P	**Arg65(HH12)**	**0.0240**	**-0.0297**	-171.72
O3P	**Arg65(HH22)**	**0.0214**	**-0.0247**	
O	Asp179(OD2)	0.0065	-0.0035	66.60
carboxylate	cation	0.0121	-0.0093	-314.87
carboxylate	cation	0.0109	-0.0040	
O3P	Gly53(HA2)	0.0024	-0.0007	13.36
O	**Ser23(HB2)**	**0.0049**	**-0.0034**	-13.04
HB1	Thr182(O-H)	0.0051	-0.0013	-41.70
OXT	**Thr182(HG1)**	**0.0211**	**-0.0254**	
OG	**Thr182(HG23)**	**0.0042**	**-0.0017**	
H1	**Asp22(OD2)**	**(*)**		16.71
H2	**Glu29(OE2)**	**(*)**		-62.54
A_w/Ca/PSer				
O	**Arg202(HH22)**	**0.0135**	**-0.0075**	-56.95
HA	Arg65(HH22)	0.0042	-0.0018	7.07
O1P	Asp22(HB2)	0.0011	-0.0004	27.35
O1P	Asp22(O)	0.0017	-0.0006	
O1P	cation	0.0131	-0.0109	-588.07
O2P	cation	0.0109	-0.0048	
O3P	Gly180(HA1)	0.0021	-0.0016	-17.17
HB2	Gly53(HA1)	0.0002	-0.0001	-4.23
O2P	**Lys158(HZ2)**	**0.0280**	**-0.0343**	-121.60
NH3	**Ser23(HG)**	**0.0032**	**-0.0015**	-9.97
phosphate	Thr182(O-H)	0.0015	-0.0004	-5.76
O	Thr48(HG22)	0.0057	-0.0031	-2.73
H3	**Glu29(OE1)**	**(*)**		-130.09
A_c/Mg/PSer				
CB	Ala61(HB2)	0.0042	-0.0009	-14.25
OG	Ala61(O)	0.0053	-0.002	
O3P	**Arg202(H12)**	**0.0366**	**-0.0478**	-201.40
O2P	**Arg202(H22)**	**0.0308**	**-0.0385**	
O2P	**Arg50(H12)**	**0.0426**	**-0.0577**	-213.72
O1P	**Arg50(H22)**	**0.0307**	**-0.0397**	
O2P	**Arg65(H12)**	**0.031**	**-0.0361**	-183.01
O1P	**Arg65(H22)**	**0.0289**	**-0.0313**	
O	Asp22(OD2)	0.0127	-0.0064	2.91
H3	**Asp22(OD1)**	**0.0012**	**-0.0000**	
O	cation	0.0404	-0.0774	-435.88
H1	Glu29(OE1)	0.0276	-0.0285	-90.48
H2	Gly111(H)	0.0002	-0.0001	1.39

OXT	**Lys158(HZ1)**	**0.0383**	**-0.0513**	-108.65
carboxylate	Thr182(HB)	0.0064	-0.0021	-14.88
HB2	Thr182(HB)	0.0127	-0.0060	
O1P	Val56(H23)	0.0034	-0.0015	-4.26
A_{cw}/Mg/PSer				
OXT	**Arg202(NH1)**	**0.0008**	**-0.0002**	-10.47
H1	Arg202(NH2)	0.0039	-0.0008	
O	**Arg49(H12)**	**0.0246**	**-0.0300**	-138.59
OXT	**Arg49(H22)**	**0.0319**	**-0.0330**	
H1	Asp179(OE2)	0.0011	-0.0002	147.95
O1P	Asp183(OD1)	0.0048	-0.0008	154.31
O3P	cation	0.0421	-0.0588	-1308.53
O1P	cation	0.0358	-0.0345	
H2	**Glu29(OE1)**	**0.0165**	**-0.0145**	-43.66
O2P	**Gly180(HA1)**	**0.0036**	**-0.0024**	0.00(1)
O1P	**Lys158(HZ1)**	**0.0159**	**-0.0113**	-124.72
P	**Thr182(O-H)**	**0.0056**	**-0.0022**	-24.61
A/Mg/PSer				
OXT	Ala51(HB3)	0.0008	-0.0005	-2.19
HA	Ala61(HB1)	0.0005	-0.0003	-2.94
O	**Arg202(HH22)**	**0.002**	**-0.001**	-35.91
H1	Glu29(HB1)	0.0012	-0.0004	40.02
H2	**Glu29(OE2)**	**0.0033**	**-0.0021**	
O	Glu29(OE2)	0.0028	-0.0003	
OXT	Gly53(HA2)	0.0055	-0.0032	-18.04
HB2	Gly53(O)	0.0092	-0.0028	
OG	Gly54(HA2)	0.0018	-0.0004	-10.89
O2P	**water(HW1520)**	**0.0551**	**-0.0858**	-67.17
O3P	**water(HW1534)**	**0.0341**	**-0.0443**	-34.59
H1	water(HW1534)	0.0101	-0.0063	
O1P	**Lys158(HZ1)**	**0.0293**	**-0.0329**	-229.15
O3P	**Lys158(HZ3)**	**0.0205**	**-0.0193**	
O1P	**Thr182(HB)**	**0.0035**	**-0.002**	-32.48
B/Ca/PSer				
OG	Arg49(CB group)	0.0039	-0.0005	-150.86
O1P	**Arg49(HH21)**	**0.0426**	**-0.0607**	
O1P	**Arg49(HE)**	**0.0187**	**-0.0106**	
O2P	**Arg50(HH12)**	**0.0281**	**-0.0354**	-113.42
HB1	Arg50(NH1)	0.0052	-0.0013	
OXT	Asp179(OD1)	0.0031	-0.0017	87.88
OXT	**Asp22(HB2)**	**0.0075**	**-0.0059**	-50.94
H3	**Asp22(OD2)**	**(*)**		
OXT	cation	0.0099	-0.0116	-595.61
O2P	cation	0.0075	-0.0058	
O3P	cation	0.0070	-0.0047	
O3P	Lys158(HZ3)	0.0214	-0.0180	-172.76
O1P	**Lys158(HZ3)**	**0.0187**	**-0.0126**	
O1P	**Thr182(HG1)**	**0.0321**	**-0.0334**	-67.23
O	Thr48(HG23)	0.0005	-0.0003	-6.77
HB1	Thr48(O)	0.0097	-0.0069	
B/Mg/PSer				
H3	Arg202(H22)	0.0007	-0.0002	-1.04
OXT	**Arg49(HH21)**	**0.0550**	**-0.0824**	-139.04
O	**Arg49(HE)**	**0.0241**	**-0.0271**	
O3P	cation	0.0311	-0.0343	-1335.30
P	cation	0.1399	-0.0768	
O1P	cation	0.0279	-0.0221	
O2P	cation	0.0308	-0.0342	
H1	Glu29(OE2)	0.0006	-0.0004	-12.77
O1P	**Lys158(HZ1)**	**0.0434**	**-0.0637**	-154.14
HB2	Phe58(CD1)	0.0012	-0.0004	
HA	Phe58(CE1)	0.0016	-0.0007	-12.76
O2P	**Thr182(O-H)**	**0.0065**	**-0.0017**	-25.92

(*) Hbond not seen as a CP but detected using isocontours of s(**r**)

Table S11. Long-living hydrogen bonds formed between residues 50-55 and 202-206 as obtained from the last 200 ns of the MD simulations at 300 K and 1 bar.

	Hbond type	duration from-to (ns)
A/Ca/PSer	/	/
A_w/Ca/PSer	Met52-Gln204	100-200
	Met52-Gly53	100-200
	Met52-Gly54	200-300
A_c/Mg/PSer	Met52-Gln204	150-265
	Ala51-Gln203	150-265
A_{cw}/Mg/PSer	/	
A/Mg/PSer	Met52-Gln204	190-300
A_c/Mg	Met52-Gln204	170-300
A_{cw}/Mg	/	
B/Ca	/	
B/Mg	/	
B/Ca/PSer	Arg50-Gln204	190-300 (rare)
B/Mg/PSer	/	

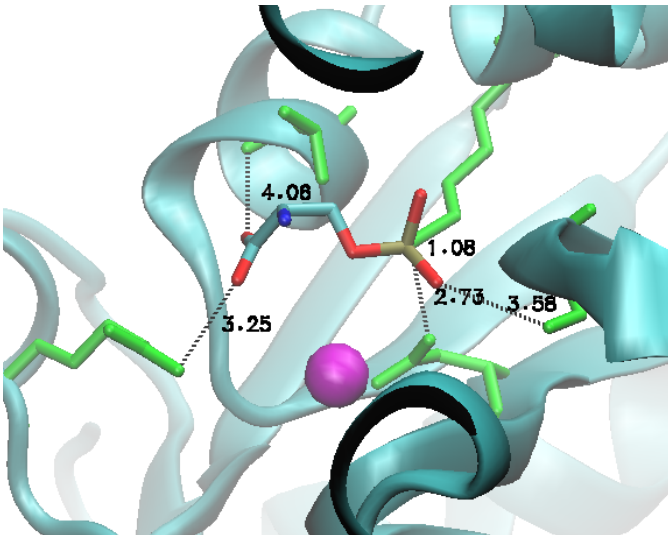

Figure S1. Crystal structure of the chain B showing close contacts between the artificially included substrate (sticks) and hPSP (cyan ribbon). Ca^{++} and the residues Asp20, Met52, Phe58, Lys158, and Thr182, are displayed in magenta and green, respectively. Distance values are in Angströms.

To place the substrate in Chain B, the crystal structure of Chain A and PSer was aligned onto the crystal structure of Chain B using the default alignment parameters of the program Pymol (Schrödinger, 2014). PSer is close to Lys158 (NZ-O2P = 0.11 nm), Asp20 (OD1-O2P = 0.27 nm), Arg202 (NH2-OXT = 0.33 nm), Ser109 (OG-O3P = 0.36 nm), and Lys182 (N-O = 0.41 nm).

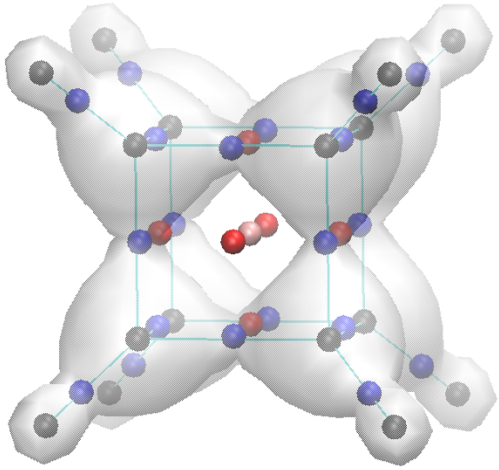

Figure S2. Critical points (peaks = black, passes = blue, pales = red, pit = pink) of the promolecular Cromer-Mann based electron density distribution for the cubane molecule (lines). The ED iso-contour value is 0.17 e/bohr^3 (light grey transparent contour).

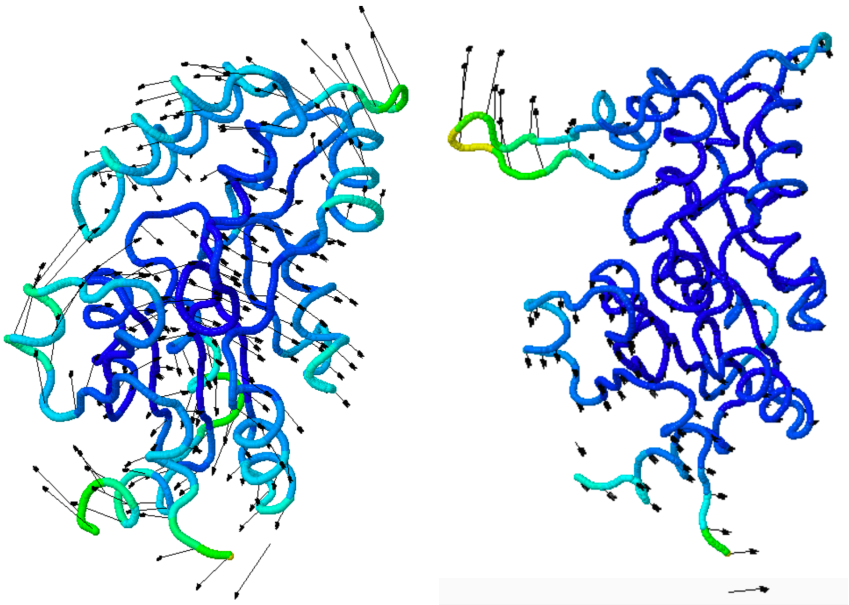

Chain A Chain B

Figure S3. Screenshots of the first vibrational mode of chains A and B of hPSP as obtained from the application of the server iMods (López-Blanco et al., 2014). The sequences are colour-coded as a function of their predicted deformability. The protein backbone colours are chosen according to the predicted mobility reported in Figure 3a.

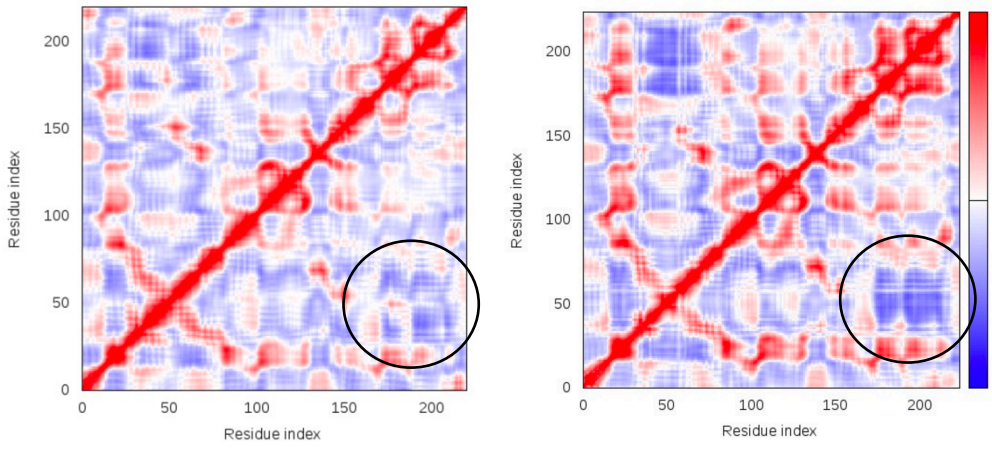

Chain A Chain B

Figure S4. Correlation matrices defined in Ref. (Ichiye & Karplus, 1991) (negative = blue, positive = red) computed using the Cα coordinates of the chains A and B of hPSP. The circles focus on the negative correlation region between both elements of the cavity aperture.

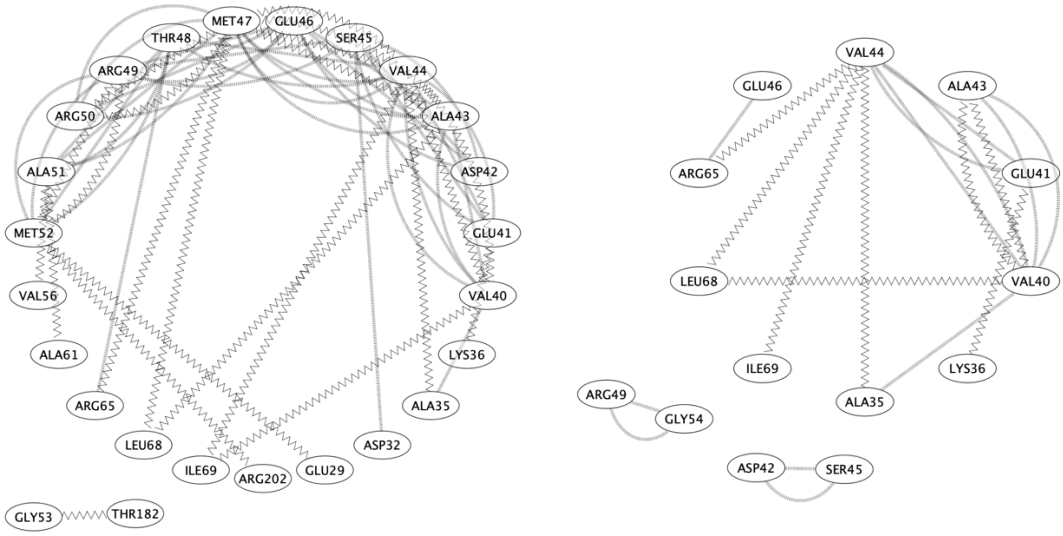

Chain A Chain B

Figure S5. Interaction networks depicting Hbonds (thick lines) and van der Waals interactions (zig-zag lines) involved by the residues 40 to 56 of the hPSP lid, as obtained by an analysis of the crystal chains A and B using RING (Piovesan et al., 2016). The RING results are displayed using the software Cytoskape (Shannon et al., 2003).

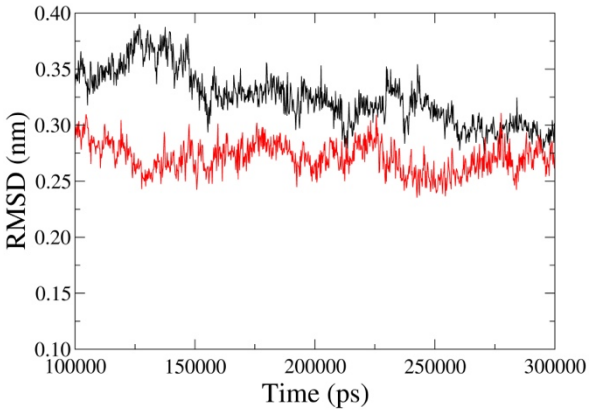

A/Ca/PSer (black), A_w/Ca/PSer (red)

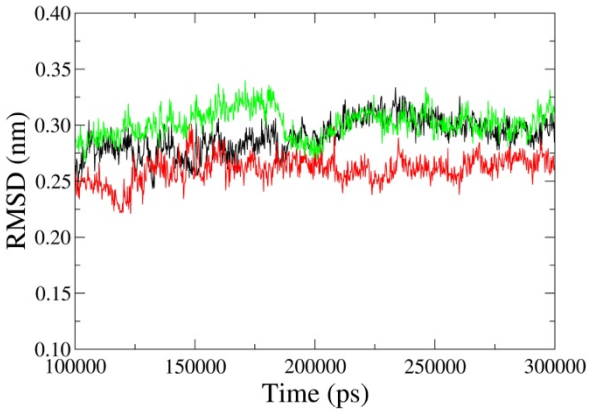

A_c/Mg/PSer (black), A_{cw}/Mg/PSer (red), A/Mg/PSer (green)

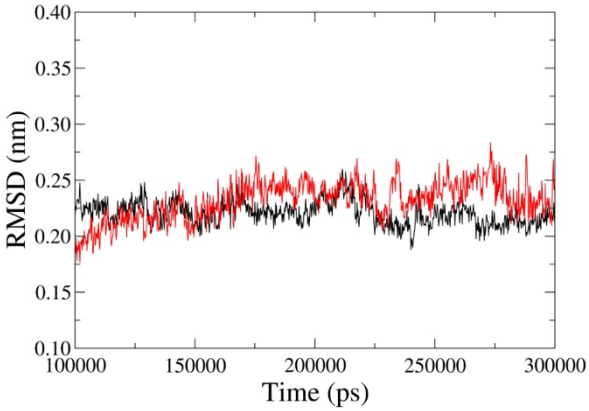

A_c/Mg (black), A_{cw}/Mg (red)

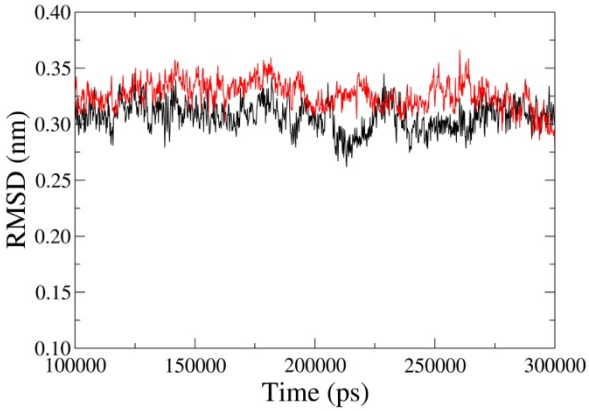

B/Ca (black), B/Mg (red)

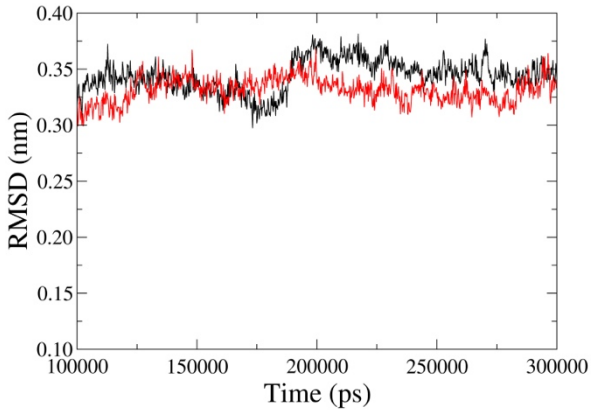

B/Ca/PSer (black), B/Mg/PSer (red)

Figure S6. RMSD of the solvated hPSP enzymes calculated versus their start conformation, as obtained from the last 200 ns of MD trajectories at 300 K and 1 bar.

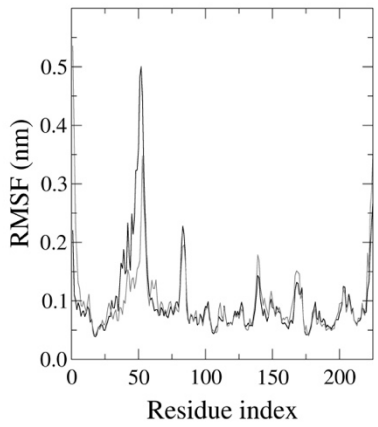

(a) A/Ca/PSer (black), A_w/Ca/PSer (grey)

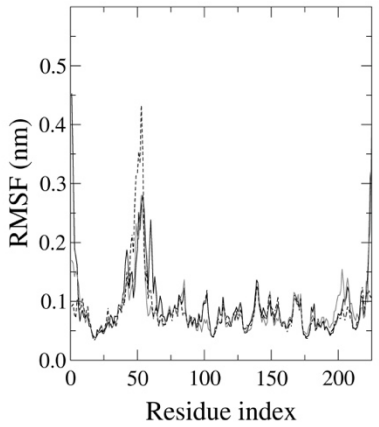

(b) A_c/Mg/PSer (black), A_{cw}/Mg/PSer (grey), A/Mg/PSer (dashed)

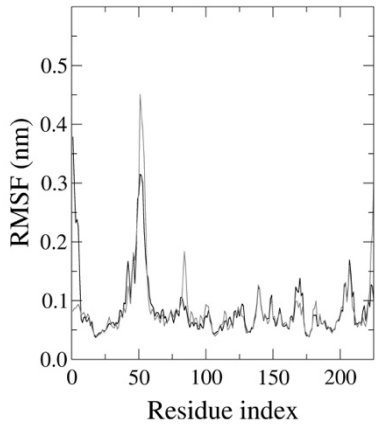

(c) A_c/Mg (black), A_{cw}/Mg (grey)

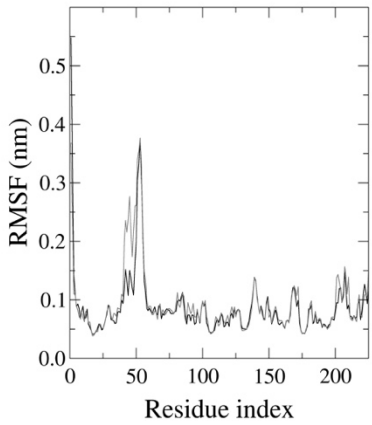

(d) B/Ca (black), B/Mg (grey)

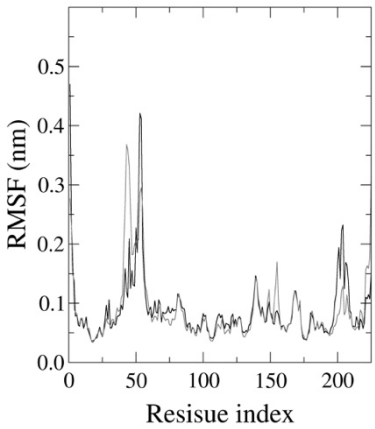

(e) B/Ca/PSer (black), B/Mg/PSer (grey)

Figure S7. RMSF of the hPSP Cα atoms as calculated from the last 200 ns of MD trajectories at 300 K and 1 bar.

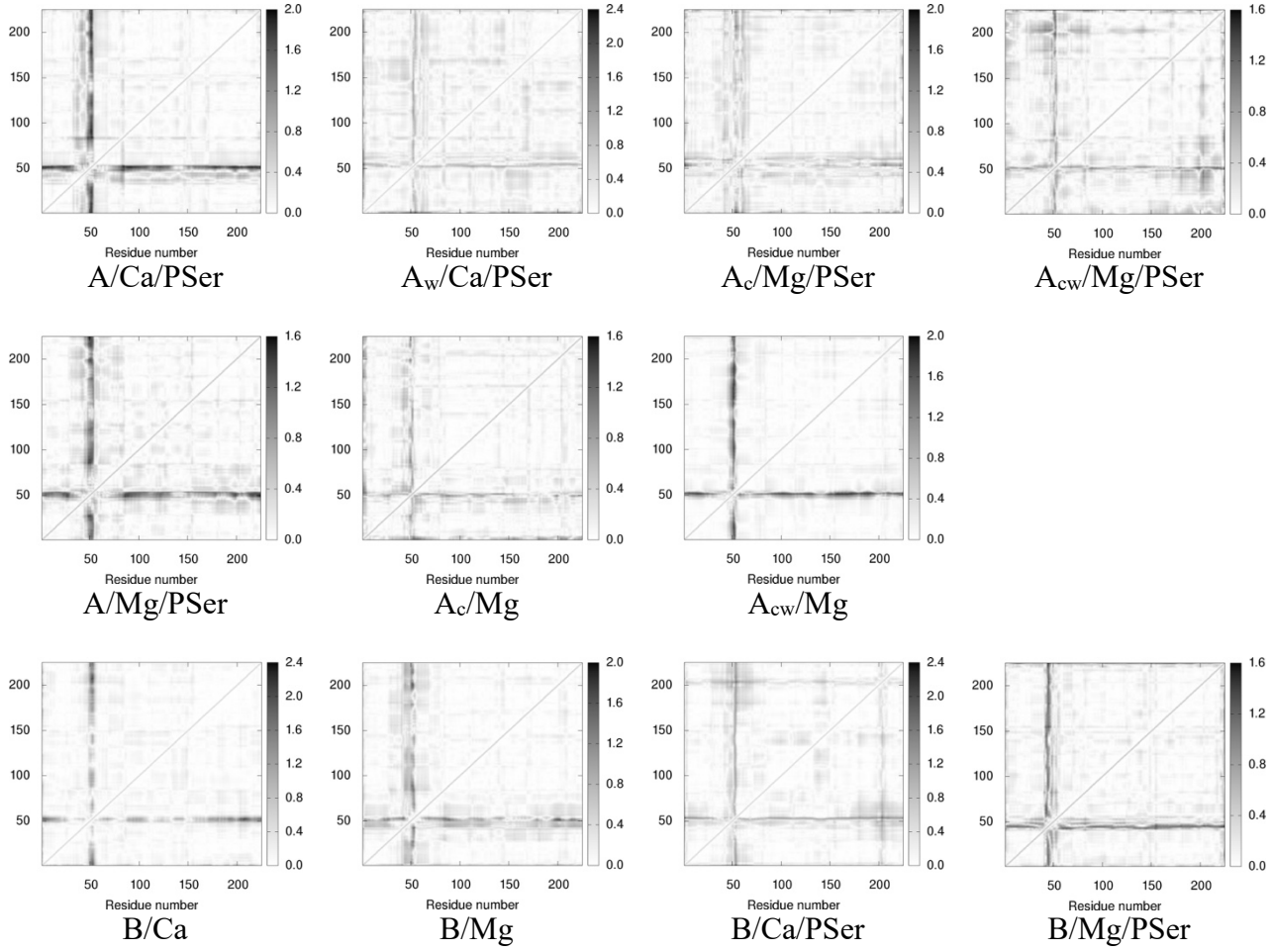

Figure S8a. hPSP $|\kappa_{ij}.\Delta d_{ij}|$ maps calculated using the first PC of the last 200 ns of MD trajectories at 300 K and 1 bar.

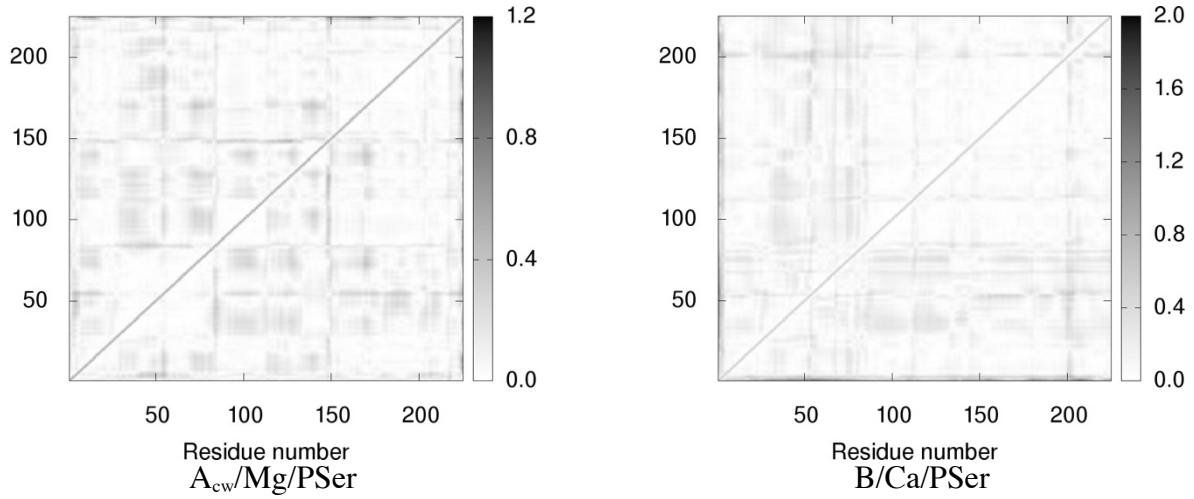

A_{cw}/Mg/PSer
Last 100 ns of the production stage

B/Ca/PSer
Last 75 ns of the production stage

Figure S8b. hPSP $|\kappa_{ij}.\Delta d_{ij}|$ maps calculated using the first PC obtained for a limited period of time of MD trajectories at 300 K and 1 bar.

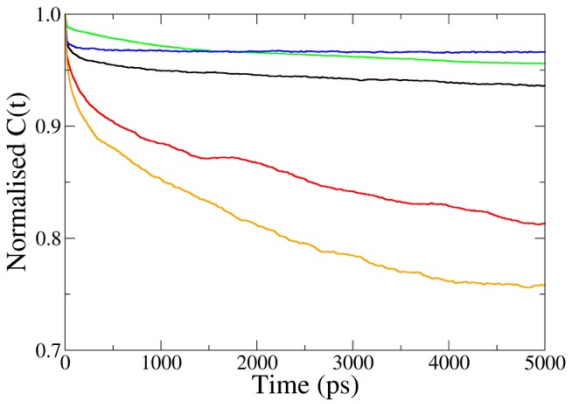

A/Ca/PSer (black), A_w/Ca/PSer (red), A_c/Mg/PSer (green), A_{cw}/Mg/PSer (blue), A/Mg/PSer (orange)

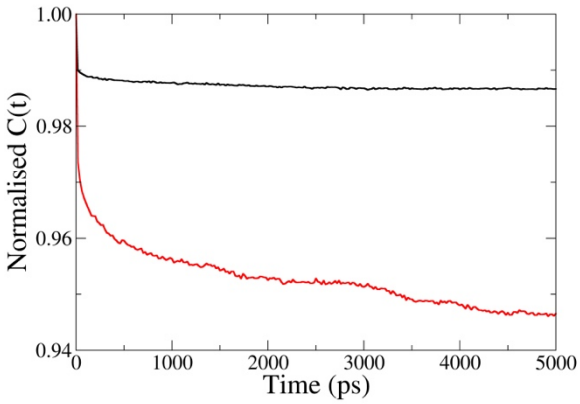

B/Ca/PSer (black), B/Mg/PSer (red)

Figure S9. First Legendre polynomial orientation autocorrelation function of the substrate PSer as obtained from the last 200 ns MD simulations at 300 K and 1 bar. Correlation times are reported in the Table below.

	τ (10^5 ps)
A/Ca/PSer	2.8
A_w/Ca/PSer	0.5
A_c/Mg/PSer	2.6
A_{cw}/Mg/PSer	38.6
A/Mg/PSer	0.3
B/Ca/PSer	40.7
B/Mg/PSer	3.8

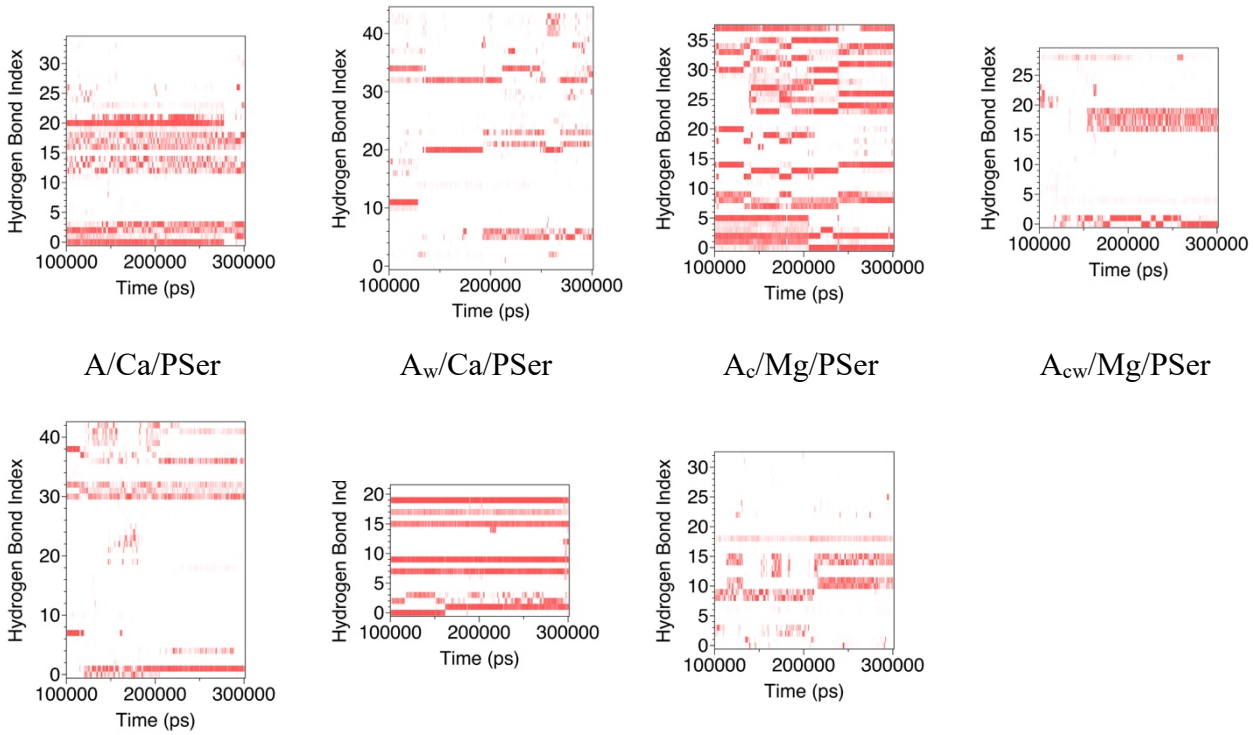

Figure S10. PSer-hPSP hydrogen bond maps as obtained from the last 200 ns of MD simulations at 300 K and 1 bar.

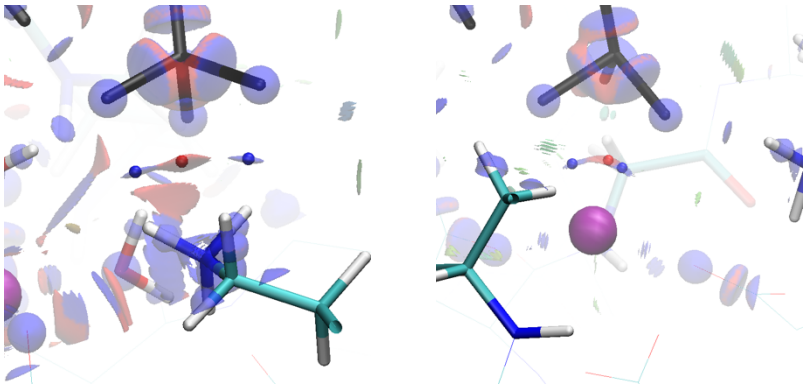

(b) Salt bridge PSer(phosphate)-Lys158 A/Mg/PSer

(c) Electrostatic PSer(phosphate)-Ion A_w/Ca/PSer

Figure S11. PSer (black sticks), selected passes (blue spheres) and pales (red spheres) superimposed to the 0.3 $e^{-1/3}$ isocontour of the RDG (negative (blue) and positive (red) transparent isosurfaces).

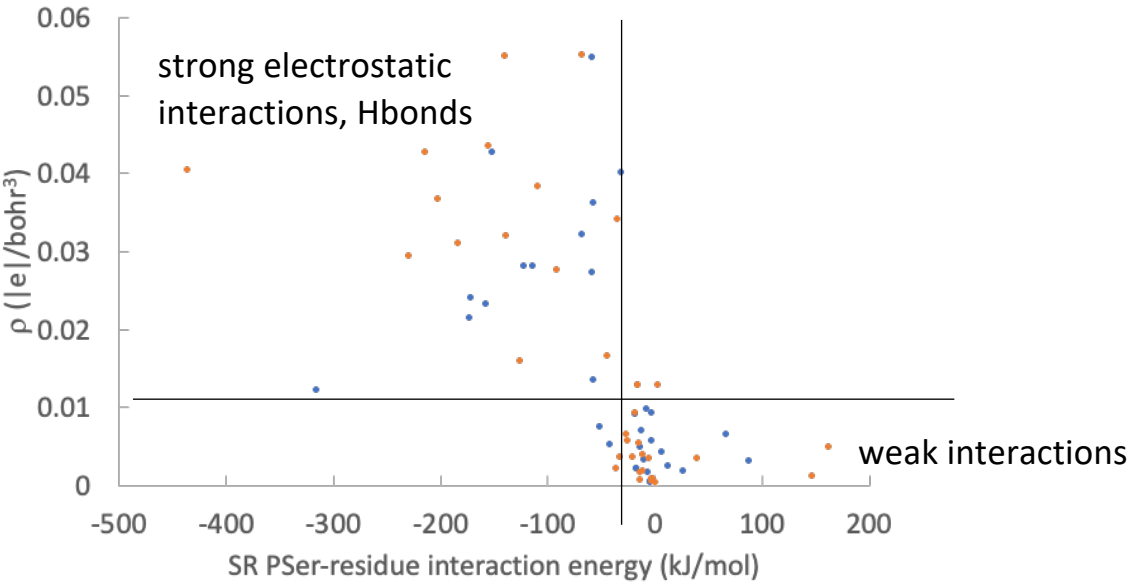

Figure S12. ED magnitude of the passes as a function of the corresponding SR interaction energy PSer-hPSP residue. Ca^{++}-dependent systems (blue), Mg^{++}-dependent systems (orange). See Table S10 for additional details. Extremely low SR interaction energies, below -10^3 kJ/mol, are not included in the Figure for the sake of clarity.

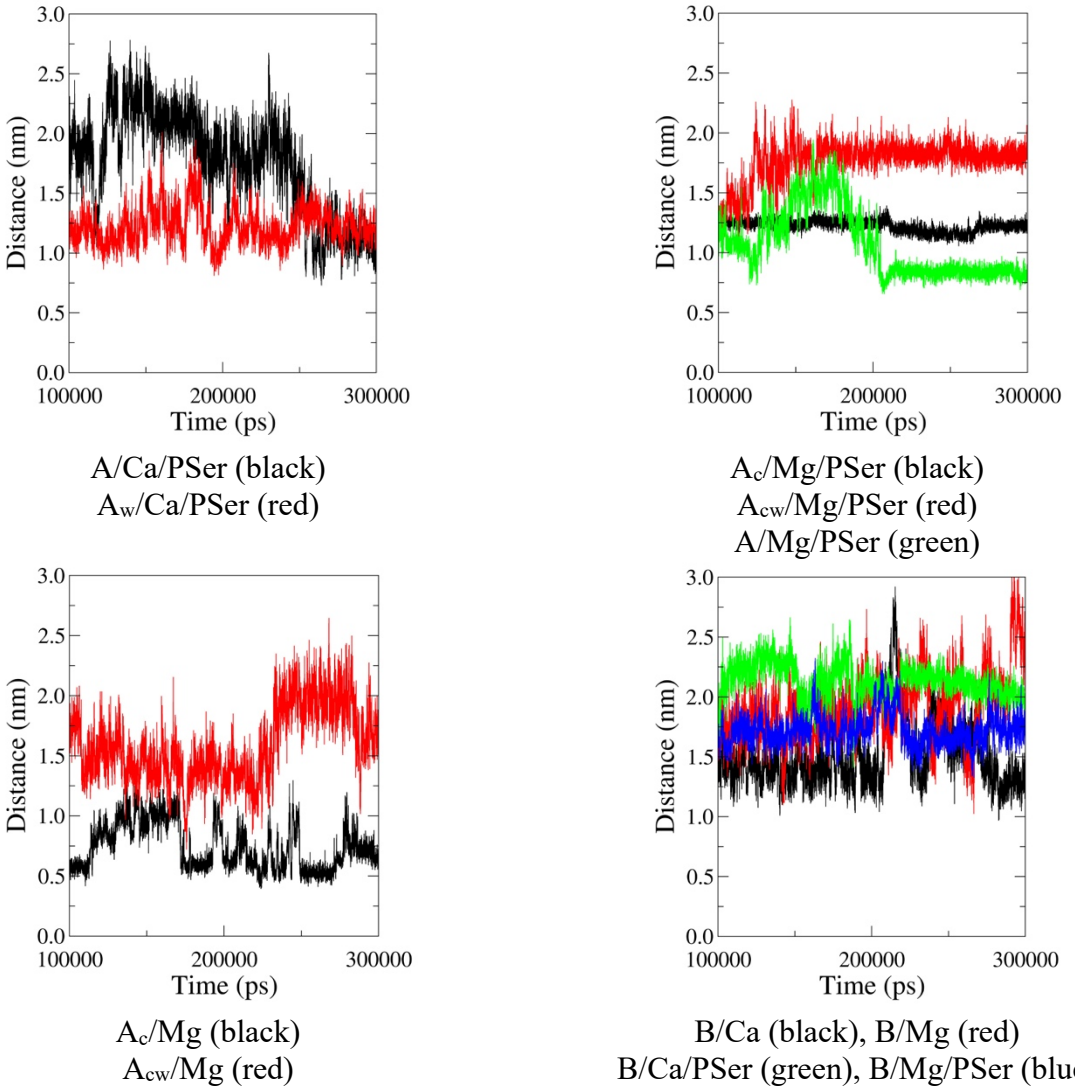

Figure S13. Distance profiles Cα52-Cα202 as obtained from the last 200 ns of MD simulations at 300 K and 1 bar.

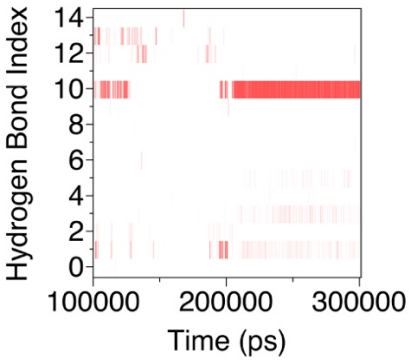

Figure S14. Profile of the hydrogen bonds occurring between amino acid sequences 50-55 and 202-206 for the system A/Mg/PSer as obtained from the last 200 ns of the MD simulation at 300 K and 1 bar.

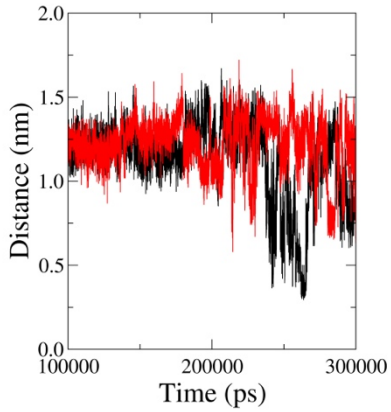

A/Ca/PSer (black); A_w/Ca/PSer (red)

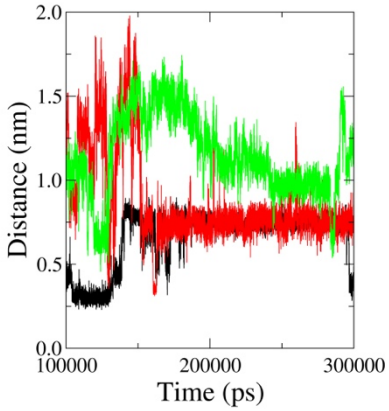

A_c/Mg/PSer (black); A_{cw}/Mg/PSer (red)
A/Mg/PSer (green)

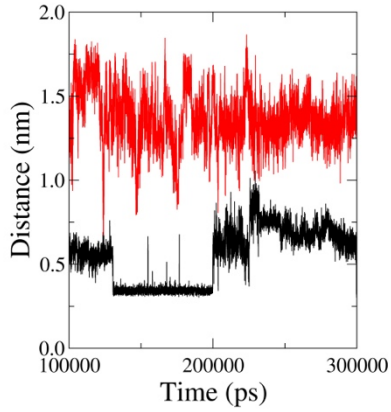

A_c/Mg (black); A_{cw}/Mg (red)

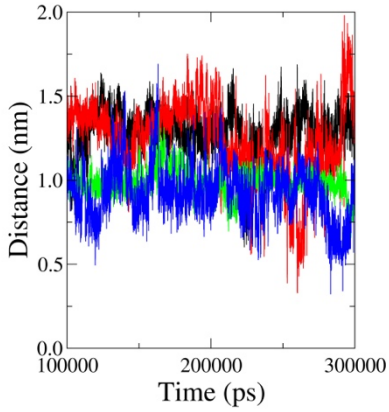

B/Ca (black); B/Mg (red)
B/Ca/PSer (green); B/Mg/PSer (blue)

Figure S15. Profiles of the minimum distance between CZ of Arg49 or Arg50 and Glu29, as obtained from the last 200 ns of MD simulations at 300 K and 1 bar.

References

Besler B. H., Merz K. M. Jr. & Kollman P. A. (1990) Atomic charges derived from semiempirical methods. *Journal of Computational Chemistry*, *11*(4):431-439.

Borodin O. & Smith G. D. Force field fitting toolkit. The University of Utah. http://www.eng.utah.edu/~gdsmith/fff.html. (last accessed 26 Aug. 2009).

Darré L., Tek A., Baaden M. & Pantano S. (2012). Mixing atomistic and coarse grain solvation models for MD simulations: Let WT4 handle the bulk. *Journal of Chemical Theory and Computation*, *8*(10):3880-3894.

Darré L., Machado M. R., Brandner A. F., González H. C., Ferreira S. & Pantano S. (2015). SIRAH: A structurally unbiased coarse-grained force field for proteins with aqueous solvation and long-range electrostatics. *Journal of Chemical Theory and Computation*, *11*(2),723-739.

Frisch M. J., Trucks G. W., Schlegel H. B., Scuseria G. E., Robb M. A., Cheeseman J. R., Scalmani G., Barone V., Mennucci B., Petersson G. A., Nakatsuji H., Caricato M., Li X., Hratchian H. P., Izmaylov A. F., Bloino J., Zheng G., Sonnenberg J. L., Hada M., Ehara M., Toyota K., Fukuda R., Hasegawa J., Ishida M., Nakajima T., Honda Y., Kitao O., Nakai H., Vreven T., Montgomery J. A. Jr., Peralta J. E., Ogliaro F., Bearpark M., Heyd J. J., Brothers E., Kudin K. N., Staroverov V. N., Kobayashi R., Normand J., Raghavachari K., Rendell A., Burant J. C., Iyengar S. S., Tomasi J., Cossi M., Rega N., Millam J. M., Klene M., Knox J. E., Cross J. B., Bakken V., Adamo C., Jaramillo J., Gomperts R., Stratmann R. E., Yazyev O., Austin A. J., Cammi R., Pomelli C., Ochterski J. W., Martin R. L., Morokuma K., Zakrzewski V. G., Voth G. A., Salvador P., Dannenberg J. J., Dapprich S., Daniels A. D., Farkas O., Foresman J. B., Ortiz J. V., Cioslowski J. & Fox D. J. (2009). Gaussian 09, Revision A.02, Gaussian, Inc., Wallingford CT.

Gonzáles H. C., Darré L. & Pantano S. (2013). Transferable mixing of atomistic and coarse-grained water models. *The Journal of Physical Chemistry B*, *117*(46),14438-14448.

Haufroid M., Mirgaux M., Leherte L. & Wouters J. (2019). Crystal structures and snapshots along the reaction pathway of human phosphoserine phosphatase. *Acta Crystallographica D*, *75*,592-604.

Hess B., Kutzner C., van der Spoel D. & Lindahl E. (2008). GROMACS 4: Algorithms for highly efficient, load-balanced, and scalable molecular simulationI *Journal of Chemical Theory and Computation*, *4*(3),435-447.

Homeyer N., Horn A. H. C., Lanig H. & Sticht H. (2006). AMBER force-field parameters for phosphorylated amino acids in different protonation states: phosphoserine, phosphothreonine, phosphotyrosine, and phosphohistidine. *Journal of Molecular Modeling*, *12*(3),281-289.

Humphrey W., Dalke A. & Schulten K. (1996). VMD - Visual Molecular Dynamics. *Journal of Molecular Graphics*, *14*(1),33-38.

Ichiye T. & Karplus M. (1991). Collective motions in proteins: A covariance analysis of atomic fluctuations in Molecular Dynamics and normal mode simulations. *Proteins*, *11*(3),205-217.

Leherte L. (2004). Hierarchical description of protein structure fragments obtained from analyses of promolecular electron density distributions. *Acta Crystallographica A*, 60,1254-1265.

Leherte L. (2016). Reduced point charge models of proteins: Assessment based on molecular dynamics simulations. *Molecular Simulation*, *42*(4):289-304.

Lindorff-Larsen K., Piana S., Palmo K., Maragakis P., Klepeis J. L., Dror R. O. & Shaw D. E. (2010). Improved side-chain torsion potentials for the Amber ff99SB protein force field. *Proteins*, *78*(8),1950-1958.

López-Blanco J. R., Aliaga J. I., Quintana-Ortí E. S. & Chacón P. (2014) iMODS: Internal coordinates normal mode analysis server. *Nucleic Acids Research*, *42*,W271-276. http://imods.chaconlab.org/ (last accessed 22 Sept. 2019).

Machado M. Tutorial 2. SIRAH forcefield in GROMACS, hybrid solvation: Plugging SIRAH solvent to your atomistic system. https://training.vi-seem.eu/images/trainingMaterial/LifeSciences/Tutorial_2_sirah4gmx.pdf (last accessed 27 Jun. 2018).

Peeraer Y., Rabijns A., Collet J.-F., Van Schaftingen E. & De Ranter C. (2004). How calcium inhibits the magnesium-dependent enzyme human phosphoserine phosphatase. *European Journal of Biochemistry*, *271*(16),3421-3427.

Pedretti A., Villa L. & Vistoli G. (2004). VEGA - An open platform to develop chemo-bio-informatics applications, using plug-in architecture and script programming. *Journal of Computational Aided Molecular Design*, *18*(3),167-173.

Piovesan D., Minervini G. & Tosatto S. C. E. (2016). The RING 2.0 web server for high quality residue interaction networks. *Nucleic Acids Research*, *44*,W367-374.

Pronk S., Páll S., Schulz R., Larsson P., Bjelkmar P., Apostolov R., Shirts M. R., Smith J. C., Kasson P. M., van der Spoel D., Hess B. & Lindahl E. (2013). GROMACS 4.5: A high-throughput and highly parallel open source molecular simulation toolkit. *Bioinformatics*, *29*(7),845-854.

Ray B. D. (2009). Topolbuild 1.3, IUPUI Physics Dept., Indianapolis IN. http://www.gromacs.org/Downloads/User_contributions/Other_software (last accessed 12 Dec. 2018).

Ryu J., Lee M., Cha J., Laskowski R. A., Ryu S. E. & Kim D.-S. (2016). BetaSCPWeb: side-chain prediction for protein structures using Voronoi diagrams and geometry prioritization. *Nucleic Acids Research*, *44*,W416-W423.

Salentin S., Schreiber S., Haupt V. J., Adasme M. F. & Schroeder M. (2015). PLIP: fully automated protein–ligand interaction profiler. *Nucleic Acids Research*, *43*(W1),W443-W447.

Schrödinger, LLC (2014). The PyMOL Molecular Graphics System, Version 1.7.4.

Shannon. P., Markiel A., Ozier O., Baliga N. S., Wang J. T., Ramage D., Amin N., Schwikowski B., & Ideker T. (2003). Cytoscape: A software environment for integrated models of biomolecular interaction networks. *Genome Research*, *13*(11),2498-2504.

Singh U. C. & Kollman P. A. (1984). An approach to computing electrostatic charges for molecules. *Journal of Computational Chemistry*, *5*(2),129-145.

Steinbrecher T., Latzer J. & Case D. A. (2012). Revised AMBER parameters for bioorganic phosphates. *Journal of Chemical Theory and Computation*, *8*(11),4405-4412.